CHAPTER 4: THE SFBR EARTHQUAKE SOURCE MODEL: MAGNITUDES AND LONG-TERM RATES

Introduction: Calculating Rupture Source Rates in a Complex Model

The tectonically complex San Francisco Bay Region (SFBR) contains both known and unidentified faults that produce a broad range of earthquake sizes at different rates of occurrence. In this chapter we use fault zone information developed in the previous chapter to construct an earthquake source model that describes long-term rates of earthquake production in the SFBR. Specifically, this *SFBR earthquake model* defines the sizes and locations of earthquake rupture sources in the region, the magnitudes of the earthquakes produced by those sources, and the long-term recurrence rates of those earthquakes. The earthquakes described by the model include large segment-breaking and floating events on the seven characterized faults, and background events on uncharacterized or unknown faults. The SFBR earthquake model is constructed using the variety of geologic, geodetic, and seismic data summarized in the previous chapter, and is faithful to what is currently known about the rates of seismic moment accumulation and release across the region.

Mean rates of earthquake occurrence are primary inputs into the calculations of earthquake probability presented in the following chapters. Information on earthquake recurrence times is limited because of the shortness of the historical and paleoseismic records. However, estimates of geologic slip rates allow us to estimate rates of seismic moment release on each of the characterized faults. There is also information on segment lengths, widths, and seismogenic scaling factors *R*, which provide an estimate of the seismogenic areas *A* of each rupture source (**Figure 2.3**). These area estimates are the basis for estimating the magnitude **M** of earthquakes that occur on them, through **M**–log *A* relations. The main focus of this chapter is the estimation of earthquake rates, which is obtained from the moment release rate and the size of earthquakes that release the moment.

If each fault segment in the SFBR acted as an independent rupture source, the calculation of earthquake rates would be straightforward: the long-term slip rate for each segment would be achieved by a repeating sequence of similar-sized earthquakes. Given the long-term moment release rate of the segment, $\dot{M}_0$ (obtained from its seismogenic area and slip rate) and the mean moment of those repeating earthquakes, $\overline{M}_0$(obtained from its seismogenic area), their ratio would define the rate of earthquakes, or *rupture source rate*, γ:

$$\gamma = \frac{\dot{M}_0}{\overline{M}_0} \qquad (4.1)$$

However, our model allows segments to fail in combination, such that the long-term earthquake history of a fault segment may involve failure in a number of different rupture scenarios involving combinations with its neighbors or failure of portions of the fault system in floating earthquakes. Also, we specify that a small fraction of the fault system's moment budget, F_{small}, goes toward the production of smaller (sub-segment sized) earthquakes. Because each fault may pro-

duce such a variety of earthquakes, we modify equation (4.1) to define a system of equations, one for each characterized rupture source, that together satisfy the long-term slip rates of all the fault segments:

$$\gamma_{char_i} = \frac{\dot{M}_{0_i} F_{char}}{\overline{M}_{0char_i}} \qquad (4.2a)$$

where subscript *char* refers to *characterized* (fixed and floating) rupture sources, $\dot{M}_{0_i}$ is the moment rate of rupture source *i*, $\overline{M}_{0char_i}$ is the mean moment of earthquakes produced by rupture source *i*, and F_{char} is the fraction of seismogenic moment rate expended in characterized earthquakes. Equation (4.2a) corresponds to the right-most box in the calculation flow diagram **Figure 2.10**. In the first three major sections that follow, we summarize the approach taken by WG02 to calculate the three quantities on the right side of (4.2a).

For the purpose of calculating large-earthquake rates—the primary purpose of this chapter—we need only discover the moment rate fraction F_{char} and other quantities in (4.2a). However, estimating F_{char} will require us to also estimate the moment rate fraction expended in aftershocks, $F_{aftershock}$, and that expended in other small earthquakes on the fault system, F_{small}, such that $F_{char} + F_{aftershock} + F_{small} = 1$. It turns out to be useful in some applications to specify the rate and magnitude distribution of those smaller events. For that purpose one may employ an expression analogous to (4.2a) for the rate of smaller earthquakes within a specified magnitude range:

$$\gamma_{small_i} = \frac{\dot{M}_{0_i} F_{small}}{\overline{M}_{0small_i}} \qquad (4.2b)$$

where $\overline{M}_{0small_i}$ is the mean moment of smaller earthquakes (within that magnitude range), and F_{small} is the fraction of seismogenic moment rate expended in smaller earthquakes. We expand briefly upon this application later in the chapter (see box later in this chapter).

Calculations are carried out independently for each of the seven characterized fault systems. We also estimate the rate of *background earthquakes* (those which occur elsewhere than on the seven characterized ones). Finally, the rates of earthquakes on the fault systems and the background are combined to find the long-term earthquake rate (as a function of magnitude) for the SFBR as a whole. Calculations were performed using a computer program that is released with this report; interested readers are directed to **Appendix G**.

Readers who wish to skip directly to the results of this analysis may turn to the section entitled "Results: Long-term earthquake rates in the SFBR" later in this chapter. There, the results of the WG02 earthquake source model calculations are presented in two tables: **Table 4.8** presents long-term rates of rupture and mean magnitudes for each fixed and floating rupture source. **Table 4.9** contains calculated earthquake occurrence rates and recurrence intervals for each fault segment. In the final sections of this chapter, the modeled values for regional, fault, and segment recurrence are evaluated by comparison to historical seismicity and paleoseismic recurrence observations in the SFBR, and to the results from other earthquake models.

Steps in the Calculation Sequence

The SFBR model is developed using the calculation steps summarized in the following chart. The first four steps collect the information needed to calculate rupture source rates from equation (4.2a). The remaining three steps complete the description of the SFBR earthquake model.

Table 4.1. Steps in the calculation sequence for the SFBR earthquake model:

Calculation step:	Strategy and equations:	Outputs:
Calculate the mean moments of characterized rupture sources, $\overline{M}_{0char_i}$ in (4.2a).	a. Calculate the mean magnitude $\overline{\mathbf{M}}_{char}$ as a function of seismogenic area A using **M**–log A relations, (4.4)-(4.6). b. Define variability of **M** as Gaussian, and determine the degree of variability, σ_m. c. Calculate $\overline{M}_{0char_i}$ as a function of $\overline{\mathbf{M}}_{char}$ and σ_m, (4.7).	Values of A and **M** are listed in **Table 4.4**.
2. Calculate rupture source moment rates, $\dot{M}_{0_i}$ in (4.2a).	a. Calculate the fault segment moment rates as a function of A and v (4.8). b. Adjust parameters in fault rupture model (**Chapter 3**) to balance the long-term moment rate of each fault segment, **Appendix G**. c. Use fault rupture models to calculate relative rupture source rates. d. Combine results to obtain $\dot{M}_{0_i}$.	Values of $\dot{M}_{0_i}$ are computed for each rupture source.
3. Determine moment rate fractions, F_{char} and F_{small}.	a. Analyze historical seismicity on SFBR faults (**Table 4.6**) to determine F_{small}. b. Determine fraction of fault moment rate expended in aftershocks, $F_{aftershock}$. c. Calculate $F_{char} = 1 - F_{small} - F_{aftershock}$.	F_{small} determined to be 0.06 [0.04 to 0.08, 95%]. $F_{aftershock}$ determined to be small and set to zero.
4. Calculate mean rate of characterized earthquakes, γ_{char} on each rupture source and on each fault segment.	a. Apply equation (4.2a) to obtain the failure rate of each rupture source. b. For each fault segment, sum the rates of all rupture sources that involve the segment.	Rupture source rates are shown in **Table 4.8**. Fault segment occurrence rates are shown in **Table 4.9**.
5. Calculate the long-term frequency-magnitude relation for each fault.	For each magnitude increment within the range of interest, sum the rates of each rupture source (4.9), (4.10).	Results are plotted in **Figures 4.6** and **4.8**.
6. Estimate the frequency-magnitude distribution of background earthquakes.	For each magnitude increment within the range of interest, calculate background rate (4.13).	Results are plotted in **Figures 4.6** and **4.8**.

Estimating the magnitudes and moments of earthquakes

The goal of this part of the calculation sequence is to determine the mean moment of characteristic earthquakes, $\overline{M}_{0char}$ for each rupture source. We first determine the mean earthquake magnitude, $\overline{\mathbf{M}}_{char}$ and define the natural variability of magnitude as a distribution around that mean. Then we calculate the mean moment from that distribution.

For earthquakes on fixed rupture sources, a mean earthquake magnitude is calculated from the seismogenic area of its rupture source. For floating earthquakes, the mean magnitude was set *a priori* (**Chapter 3**). For both types of earthquakes, we allow for natural variability in earthquake magnitude (for a given rupture area) by describing the magnitude as a probability density function with truncated normal distribution (**Figure 4.1**). Once the mean magnitude and distribution function are in hand, it will be straightforward to calculate the mean moment of repeated earthquakes on each rupture source from equation (4.7).

Seismogenic area

The *seismogenic area* is the effective portion of fault surface that produces earthquakes

$$A = LWR. \qquad (4.3)$$

L is segment length, the distance between two segmentation points (**Figure 2.5**). *W* is down-dip segment width, corresponding to the thickness of the brittle upper crust in which strain energy available to be released as earthquakes is stored. *R* is a *seismogenic scaling factor* (ranging from 0 to 1) that accounts for the role of fault creep in reducing the fault surface area available for earthquake rupture. These quantities are further described in Chapter 3, and tabulated for each fault segment in **Table 3.8**.

The seismogenic area of a rupture source is sum of seismogenic areas of the fault segments which comprise it. Rupture source areas are listed in **Table 4.4**, along with the mean magnitudes calculated in the following section.

Mean characteristic magnitude.

Following the findings of Wells and Coppersmith (1994), we utilize **M** – log *A* relations to obtain mean magnitude of characteristic earthquakes, where *A* is seismogenic area. From regression of data for 83 continental strike-slip earthquakes, Wells and Coppersmith (1994) found (their Table 2A and Figure 16a):

$$\mathbf{M} = (3.98 \pm 0.07) + (1.02 \pm 0.03) \log_{10} A, \qquad (4.4)$$

where *A* has units of km^2. The regression is well determined, as indicated by the small standard errors (± one sigma) for the regression coefficients. However, WG99 noted that equation (4.5) significantly underestimates **M** for large (**M** ≥ 7) strike-slip earthquakes in California, **Figure 4.2a**. For their report, WG99 assembled from several sources larger data sets for global strike slip earthquakes. Those data appear in **Appendix D**, accompanied by a brief analysis of likely

measurement uncertainties in **M** and *A*. There is considerable uncertainty in the data available for the correlation analysis that we rely upon for our estimates of **M**. Therefore, two different approaches were followed to develop new relations consistent with available data in the magnitude range of primary interest in this report.

In the first approach, the data $A > 500$ km^2 were fitted with simple, one-parameter equations:

$$\mathbf{M} = 4.1 + \log_{10} A \quad (4.5a)$$
$$\mathbf{M} = 4.2 + \log_{10} A \quad (4.5b)$$
$$\mathbf{M} = 4.3 + \log_{10} A \quad (4.5c)$$

The preferred equation (4.6b) is obtained from maximum likelihood fitting of the data with coefficient on the logarithm held fixed at 1.0. For $\mathbf{M} \geq 6.7$, (4.5b) fits the data well, with an r.m.s. error of 0.19 for $A > 500$ km^2 (**Figure 4.2e**). Although this relation over-predicts **M** for $A < 500$ km^2, the measured rupture areas of those earthquakes may be biased, particularly by the use of aftershock area as a measure of rupture area by Wells and Coppersmith (1994). (See Mendoza and Hartzell (1987) for a discussion of the systematics of aftershock areas and rupture areas.) Equations (4.5a) and (4.5c) represent approximately 95% bounds on the fit (**Figures 4.2d** and **4.2f**).

Hanks and Bakun (2001) took a different approach. For $\mathbf{M} < 7$, where the Wells and Coppersmith (1994) relations work well, Hanks and Bakun (2001) noted that they could be reproduced theoretically using constant stress drop ($\Delta\sigma$) source scaling, with $\Delta\sigma$=30 bars. For $\mathbf{M} \geq 7$, they invoked *L*-model (length) scaling of average fault slip $U=\alpha L$, where $\alpha=2 \times 10^{-5}$, found elsewhere in Wells and Coppersmith (1994). The Hanks and Bakun (2001) model for converting segment and multi-segment areas to **M** comes in the form of two pairs of equations (**Figure 4.2b,c**), each expressing a bilinear relation between **M** and *A* above and below some area threshold:

$$\mathbf{M} = 4.03 + \log_{10} A \ (A \leq 1000 \text{ km}^2), \quad \mathbf{M} = 3.03 + 4/3 \log_{10} A \ (A > 1000 \text{ km}^2) \quad (4.6a)$$

and

$$\mathbf{M} = 3.98 + \log_{10} A \ (A \leq 468 \text{ km}^2), \quad \mathbf{M} = 3.09 + 4/3 \log_{10} A \ (A > 468 \text{ km}^2). \quad (4.6b)$$

Equations (4.6a) are purely a model construct, based on $\Delta\sigma$=30 bars and $\alpha=2 \times 10^{-5}$. Equations (4.6b) result from least-squares adjustments of the intercept values (but not the slopes), yielding a best-fitting $\Delta\sigma$=26 bars and $\alpha=2.3 \times 10^{-5}$. The r.m.s. error is 0.21 for $A > 500$ km^2.

Branch weights for the six candidate **M**–log *A* models, above, were obtained through a vote of the WG02 Overview Group (OG), following extensive discussion of the relative merits of each of the six equations above. Consideration was given to the magnitude, slip, and recurrence interval implied by each equation, particularly for the San Andreas and Hayward/Rodgers Creek fault systems for which paleoseismic and historical data are available. Opinions varied considerably on the importance to be place on matching the observed magnitude and slip of the 1906 San Andreas earthquake. There emerged two, very different views on this issue: (1) that the 1906 earthquake is one instance in a global dataset, in which it sits near the bottom in **M**–log*A* space for $\mathbf{M} \geq 7.5$ continental strike-slip earthquakes, or (2) that the 1906 earthquake is a dataset of one—but the one such earthquake we know to be relevant to SFBR. In the latter way of looking at the

1906 earthquake, the 1906 earthquake is indeed in a league of its own, with considerably longer rupture than even its southern California cousin, the 1857 Fort Tejon event, of comparable **M** but far shorter fault length.

For some perspective on where the 1906 event sits with regard to **M** vs *L*, a short table of data for large continental strike-slip earthquake follows.

Table 4.2. Magnitudes and rupture lengths for selected continental strike-slip earthquakes.

Year	Earthquake	Magnitude	Length (km)
1857	Fort Tejon	M7.9	300
1905	Bulnay, Mongolia	M8.0-8.1	300-350
1906	San Francisco	M7.8	480
1920	Kansu, China	M8.0	220
1939	Erzihcan, Turkey	M7.9	330-360
1957	Gobi-Altay, Mongolia	M7.8-8.1	260

Opinion was nearly evenly divided within the OG on these two ways at looking at the 1906 earthquake.

Members of the WG02 Oversight Group were polled on the relative likelihood of each relation. Resulting weights were rounded to increments of 0.05, and equation (4.5c), which received little support, was abandoned. Results are shown in **Table 4.3**. These models and model weights supersede those developed by WG99.

Table 4.3: Expert-opinion weights of **M**–log *A* models.

Equation #	Mean voted weight	Adopted weight
(4.4)	0.138	0.15
(4.5a)	0.229	0.25
(4.5b)	0.377	0.40
(4.5c)	0.033	0
(4.6a)	0.150	0.15
(4.6b)	0.073	0.05

Table 4.4. Areas, mean magnitudes of SFBR rupture sources.

		Seismogenic area (km^2) (km^2)			Mean magnitude		
Fault Name	Rupture Source	Mean	2.5%	97.5%	Mean	2.5%	97.5%
San Andreas	SAS	829	606	1141	7.03	6.84	7.22
	SAP	1066	765	1483	7.15	6.95	7.32
	SAN	2042	1545	2678	7.45	7.28	7.61
	SAO	1434	1093	1817	7.29	7.12	7.44
	SAS+SAP	1907	1483	2412	7.42	7.26	7.56
	SAP+SAN	3121	2478	3815	7.65	7.48	7.79
	SAN+SAO	3482	2755	4432	7.70	7.53	7.86
	SAS+SAP+SAN	3958	3187	4779	7.76	7.59	7.92
	SAP+SAN+SAO	4559	3621	5537	7.83	7.65	8.01
	SAS+SAP+SAN+SAO	5397	4341	6531	7.90	7.72	8.10
	floating	–	–	–	6.90	6.90	6.90
Hayward/RC	HS	367	210	599	6.67	6.36	6.93
	HN	235	119	391	6.49	6.18	6.78
	HS+HN	616	400	882	6.91	6.68	7.12
	RC	736	563	949	6.98	6.81	7.14
	HN+RC	981	756	1267	7.11	6.94	7.28
	HS+HN+RC	1359	1044	1737	7.26	7.09	7.42
	floating	–	–	–	6.90	6.90	6.90
Calaveras	CS	48	1	107	5.79	0.00	6.14
	CC	132	53	353	6.23	5.75	6.68
	CS+CC	176	59	395	6.36	5.87	6.75
	CN	465	348	610	6.78	6.58	6.97
	CC+CN	616	433	861	6.90	6.68	7.11
	CS+CC+CN	657	464	921	6.93	6.72	7.14
	floating	–	–	–	6.20	6.20	6.20
	floating CS+CC	–	–	–	6.20	6.20	6.20
Concord/GV	CON	137	44	323	6.25	5.75	6.67
	GVS	131	46	285	6.24	5.75	6.65
	CON+GVS	291	111	541	6.58	6.13	6.91
	GVN	85	25	213	6.02	5.45	6.49
	GVS+GVN	235	93	439	6.48	6.03	6.81
	CON+GVS+GVN	395	182	668	6.71	6.34	7.00
	floating	–	–	–	6.20	6.20	6.20
San Gregorio	SGS	701	504	958	6.96	6.75	7.17
	SGN	1272	966	1683	7.23	7.04	7.41
	SGS+SGN	1983	1556	2513	7.44	7.27	7.58
	floating	–	–	–	6.90	6.90	6.90
Greenville	GS	311	199	460	6.60	6.37	6.83
	GN	351	225	512	6.66	6.41	6.88
	GS+GN	670	488	892	6.94	6.74	7.13
	floating	–	–	–	6.20	6.20	6.20
Mt Diablo	MTD	350	210	489	6.65	6.42	6.89

Natural variability in magnitude about its mean

For repeated ruptures of a fault of given area, one expects some variation in magnitude about its mean due to variations in factors such as earthquake stress drop. WG99 considered various distributions; this is an area rich in controversy but poor in constraining data. Lacking a firm precedent, we chose a truncated Gaussian distribution in moment magnitude, **M** (over, say, a truncated Gaussian distribution in moment), **Figure 4.1**. The variability in magnitude is approximately Gaussian when variations in magnitude arise from Gaussian variations in the length, width and mean slip, all with comparable coefficients of variation (ratio of standard deviation to the mean). Under this assumption, the corresponding variability in moment is approximately lognormal.

The aleatory (natural) variability in **M** of σ_m=0.12 magnitude units was derived by considering the influence of errors in the measurement of both **M** and rupture area, *A*, on **M**–log *A* relationships. Independent estimates of **M** and *A* for 16 strike slip earthquakes were used to estimate their epistemic uncertainty (**Appendix D**). The measurement error of **M** corresponds to a standard deviation of approximately 0.08 magnitude units. Similarly, the measurement error for log(*A*) is 0.15 log-units (a factor of 1.4). Taking the observational errors into account in plots of **M** versus log *A* (**Figure 4.2**), we find that an aleatory variation of 0.12 for **M** is consistent with available data, whereas larger values, such as 0.25 based on ignoring measurement errors, are not.

We truncate the normal distribution of **M** at ±2 standard deviations = ±0.24. In other words, we assume that a rupture source of a given area will produce earthquakes that vary in magnitude over a range of 0.48 magnitude units. This truncation prevents there from being rare earthquakes that deviate greatly from a "reasonable" magnitude for a given area and those with slips and implied stress drops far greater than those observed in nature. Again, this is consistent with the available data, but those data are insufficient to test the correctness of this treatment. (The magnitude variability implied by this truncation is illustrated graphically in several figures in **Appendix D**.)

Calculating mean moment

The mean moment of the characteristic earthquake is a function of its mean magnitude $\overline{\mathbf{M}}_{char}$ and the shape and truncation limits of the magnitude pdf. For magnitude described by a Gaussian truncated at $\pm 2\sigma_m$, the moment is approximately log-normally distributed. The mean moment is

$$\overline{M}_{0char} = \frac{1}{\sqrt{2\pi}} \int_{-2}^{2} 10^{1.5(\mathbf{M}+\sigma_m x)+16.05} e^{-\frac{x^2}{2}} dx \qquad (4.7a)$$

which can be approximated by the following expression:

$$\overline{M}_{0char} = 10^{1.5\overline{\mathbf{M}}_{char}+16.05-0.0481\sigma_m+1.775\sigma_m{}^2} \qquad (4.7b)$$

To determine the constants in (4.7b), the mean moment was estimated numerically for a range of σ_m. The ratio of the mean moment to the moment for the mean magnitude was computed for each

σ_m, then the resulting ratios were fitted to the form of equation (4.7b) using ordinary least-squares. This avoids having to compute the integral in (4.7a).

Estimating rupture source moment rates

The following calculations define the long-term rate of seismic moment release on each rupture source, $\dot{M}_{0_i}$ in equations (4.2a,b). The moment release rate for each rupture source is found by summing contributions from its component fault segments. Quantifying those contributions is not straightforward, because a given fault segment may fail in one-segment, multi-segment, and/or floating earthquakes. We must ask: How much of a fault segment's long-term moment rate is expended in each type of earthquake? For example, on a two-segment fault such as the San Gregorio, how much of each segment's moment rate is expended in one-segment, two-segment, and floating earthquakes? The slip (or moment) from those various earthquakes must balance the long-term slip rate (or moment rate) for each segment.

Three steps are taken to define the rupture source moment rates:

1) Query panels of experts for *fault rupture models* that define the relative likelihood for fault failure in various modes (this was done by WG99 as described in **Chapter 3**),
2) Calculate the available moment rate from the seismogenic area and slip rate of the fault segments, and
3) Combine a fault rupture model and fault segment moment rates to obtain a set of relative rupture source moment rates that balance the long-term slip rate.

Fault segment moment rate

Each segment is represented as a rectangular fault patch with uniform long-term slip rate (**Figure 2.5**). The moment rate of each fault segment is obtained from its seismogenic area *A* from equation (4.3) and its long-term slip rate *v*:

$$\dot{M}_0 = \mu A v \qquad (4.8)$$

where μ is shear modulus (taken here as 3×10^{11} dyne/cm^2). Values of *v* for each fault segment were developed in the previous chapter and are listed in **Table 3.8**.

Regional slip-rate (plate rate) constraint

Global Positioning System (GPS) data collected between 1992 and 2000 in central California (Prescott and others, 2001) document the deformation across the Pacific-North America plate boundary that drives the earthquake activity in the SFBR (**Figure 1.1**). Prescott and others (2001) model most of the deformation as 39.8±1.2 mm/yr (±1σ) of shear on planes parallel to the San Andreas fault system, in agreement with 39±2 mm/yr obtained by Argus and Gordon (2001) using GPS and VBLI data. A longer-term estimate, 41 ± 1 mm/yr (±1σ), was obtained by DeMets and Dixon (1999), and Prescott and others (2001) using global plate-motion models. The shear deformation is distributed across a 120-km wide zone in the SFBR that corresponds to the width of the study region. Because there are uncertainties on the long-term slip rate of each fault segment, it is possible for a SFBR source model to contain combinations of segment slip rates

that violate the region-wide geodetic constraint. Therefore, we check the viability of each candidate model by summing the chosen slip rates across three transects (**Figure 1.3**), and rejecting those models for which the sum lies outside the range 36 to 43 mm/year (**Table 4.5**). The 36 to 43mm/yr range reflects the greatest upper 2σ limit and least lower 2σ limit of the short-term GPS and longer-term plate-motion estimates of deformation. The transects cross known faults not characterized in our model (e.g., the Zayante, Sargent, Coyote Creek, Madrone Springs, and Ortigalita faults); we account for these faults by adding a small, additional slip rate (see **Table 4.5**) to the fault-segment sums before comparing to the geodetic range.

Table 4.5: Plate-motion constraint transects.

Transect	Fault segments	Added slip Rate increment	Range of possible slip rate	Percent of trials rejected*
Northern	SAN+RC+GVN	3 mm/yr	33 to 49	18%
Central	SGN+SAP+HS+CN+GN	1 mm/yr	30 to 54	33%
Southern	SGN+SAS+CC	2 mm/yr	31 to 51	19%

* Candidate model is rejected if any (at least one) transect lies outside the range 36-43 mm/year.

The plate-motion constraint rejects 18%, 33%, and 19% of the candidate aggregate models for the northern, central, and southern transects respectively. 42% of the aggregate models are rejected on the basis of at least one transect. Thus, 17,120 trials were required in order to obtain the 10,000 viable models used to obtain the results of this report.

Defining relative likelihoods of rupture

This step defines the suite of rupture sources for which earthquake magnitudes and rates will be calculated, and employs expert opinion to assign a relative likelihood of rupture to each source. Two types of rupture sources are considered: 1) *fixed rupture sources* that consist of one or more contiguous fault segments that fail together in an earthquake. 2) *floating rupture sources* that can occur anywhere along the fault.

As described in the previous chapter, the fault characterization sub-groups assigned preliminary relative likelihood to the various rupture sources by assembling *fault rupture models* for each system. A fault rupture model consists of combinations of *rupture scenarios* that define the complete rupture of the fault system (e.g., **Figure 3.2**). Each scenario is assigned a weight, or relative frequency, which specifies the amount that that mode of failure contributes to the long-term seismic behavior of the fault. Recall that the sub-groups used a combination of available evidence and expert opinion to develop alternative fault rupture models, i.e., alternative combinations of scenario frequencies. The fault rupture models were weighted collectively by expert opinion. The variation in scenario frequencies between models (e.g., across a row of **Table 3.4**) reflects the degree of certainty that exists in the community about the strength and persistence of segmentation points on each fault. In each realization of the model, a single fault rupture model (a set of relative scenario rates, e.g., a column of **Table 3.4**) is selected for each of the seven fault systems.

In general, the relative scenario frequencies within a given fault rupture model will not result in a moment-rate-balanced model (i.e., will not satisfy $\dot{M}_0$ on each fault segment) because the rupture sources within each segmentation scenario have different moments, and those moments vary

with the choices of *L*, *W* and *R* made in a given realization of the SFBR model. The problem of moment-rate balancing the model is over-determined because there are generally more rupture source rates determined from the relative scenario frequencies than segment moment rates (or slip rates) to constrain them. Therefore, we use least-squares regression to obtain a set of revised relative rates that are the best fit to the relative rates supplied by the subgroups. Details of this procedure and comments on its effectiveness are given in **Appendix G**.

Rupture source moment rate

The moment rate for each rupture source, $\dot{M}_{0_i}$ (numerator of (4.2a)) is calculated as product of the available moment rate (sum of segment moment rates (4.8)) times the moment-balanced partition factors (above), summed across all rupture scenarios that include the given rupture source.

Partitioning moment rate across earthquake types

Fault segments in our model are typically tens of kilometers in length. Because fault segments are the smallest units of the characterized faults that can rupture in the model, the set of characteristic rupture sources does not provide a complete description of independent earthquakes in the SFBR. The lower size limit on characterized earthquakes varies from fault to fault; for the region as a whole the model is incomplete below about **M**6.7. Small earthquakes on characterized faults fall into two classes: aftershocks, the occurrence of which is dependent on an earlier main shock, and those that occur on a fault system but are not part of an aftershock sequence. It is necessary to account for the fraction of fault system moment expended in such events, lest the rate of characterized earthquakes be overestimated. In the following sections we calculate the moment rate fraction expended in these two classes of earthquakes. The moment rate expended in aftershocks will be shown to be small, and will be ignored in our analysis (i.e., $F_{aftershock} \approx 0$). The moment rate fraction in small earthquakes, F_{small}, will be shown to be a few percent.

Seismic moment rate in aftershocks

Aftershocks occurring on the characterized fault plane contribute to the long-term moment budget. Their occurrence is contingent upon the recent occurrence of a main shock, and therefore cannot be considered to be independent earthquakes as are those of the other three types. However, to the extent that their occurrence contributes to the long-term moment rate of the fault, the moment due to aftershocks should be accounted for, and our model allows a fraction of the moment rate for each source to be removed. Analysis of main shock/aftershock sequences in California (**Appendix E**) demonstrates that the summed moment of aftershocks equals, on average, 10% of the main shock moment. That is a considerable fraction of the moment budget; however, that average value is held high by the occasional occurrence of a very large aftershock, typically on a fault plane other than that which hosted the main shock. Restricting the analysis to aftershocks occurring on or near the main shock plane, $F_{aftershock}$ is roughly 3±2%. The WG99 Overview Group had substantial disagreement among OG members on the relationship between aftershocks and the seismic moment rate on the parts of faults responsible for the generation of large earthquakes, in particular whether the spatial distribution of aftershock moment release on the fault plane is similar to, or complementary to, the pattern of moment release in mainshocks. Due to this lack of consensus, and because $F_{aftershock}$ is small compared to uncertainties in other parts of

the calculation sequence, we chose not to remove aftershock moment in our calculations[1]. All else being equal, removing this small moment-rate increment would have slightly lowered earthquake rates and 30-year earthquake probabilities.

Seismic moment rate in smaller earthquakes

Previous studies have examined fault and regional seismicity to determine the ratio of moment expended in characteristic events versus smaller ones. Youngs and Coppersmith (1985)separated fault seismicity into characteristic events with magnitudes distributed around a central value, and smaller earthquakes with an Gutenberg-Richter (G-R) magnitude-size distribution, or "exponential tail" (see **Figure 4.1**) Based on examination of data from several faults, they specified distribution parameters that corresponded to placing 94% of the moment in the characteristic events and 6% in the exponential tail. Similarly, Field et al. (1999) examined the moment rates in characteristic and smaller earthquakes in southern California. They found that roughly 15% moment rate in a G-R distribution of earthquakes capped at **M**=6.7 enabled the observed rates of intermediate-magnitude seismicity to be matched; this percentage was shown to be sensitive to the number of seismogenic faults contained in the model, as their model combined our "background" seismicity and small (sub-segment-sized) earthquakes on the characterized faults.

We used Wesson et al.'s (2003) analysis of 150 years of historical seismicity (Bakun, 1999) to estimate the value of F_{small} appropriate for the SFBR. The probabilities for each historical earthquake associated with each of the characterized faults and with the background are listed in Table 3 of Wesson et al. (2003). **Table 4.6** is Wesson et al's Table 3 reordered so that the earthquakes are listed in order of increasing **M** and the probabilities are multiplied by the moment for that **M**. The moment listed for the 1906 earthquake is for that part of the 1906 rupture within the SFBR (Bakun, 1999). The summed moment for all earthquakes on a fault with **M** less than some magnitude threshold M_T is easily obtained from the list.

The threshold M_T for each fault system is our minimum mean characteristic **M** less 0.24 (*i.e.*, $2\sigma_m$): M_T=6.65 for the San Andreas fault, etc. (See M_T at bottom of table.) The seismic moment rate for small earthquakes for each fault is the summed moment for events with **M**<M_T divided by 150 years. Whereas 150 years is not long enough to sample many characteristic earthquakes, it may be long enough to establish the character of smaller events on each fault. If M_T is much larger than 5.5 on a fault, then the moment for missing **M**<5.5 events can be ignored. The Calaveras fault, with M_T=5.56, does not meet this criteria, so we omit that fault from the mean estimate below. **M_0/yr** is the moment rate in the exponential tail for each fault.

The line "Model Moment/yr" in **Table 4.6** is the moment rate for the characterized segments on that fault using approximate values of fault lengths, widths, geologic slip rates, and R values. The line "% of model" is the % of seismic moment in the exponential tail = M_0/yr divided by "Model Moment/yr". For example, according to this analysis, 8.93% of the model moment rate for the SAF has been released in earthquakes **M**<6.65. Lacking a longer catalog, we assume that this percentage is typical for the fault.

[1] The WG02 computer code allows the removal of aftershock moment rate by specifying $F_{aftershock} > 0$. This moment is removed entirely from the model, thereby lowering the moment rate available for making characteristic earthquakes.

The mean % of model ± 1σ is 0.062 ± 0.010, close to the value of 0.06 obtained by Youngs and Coppersmith (1985) for the San Francisco Bay area. From this analysis, we adopt the mean ± 2σ to define branch values for F_{small} of 0.04, 0.06, and 0.08 with appropriate weights.

Note on occurrence rate of smaller earthquakes

This probability report is not concerned with the probability of small earthquakes in the region, and we do not report either the rate of small earthquakes nor the probability of their occurrence within specified time intervals. However, certain applications of our results may require that the frequency of earthquakes be specified over a broad range of magnitude. The WG02 computer code includes the provision to compute the time-independent rate of earthquakes over a specified magnitude interval. In designing this feature of the code, we follow the lead of previous authors (e.g., Youngs and Coppersmith, 1985, and Field et al., 1999) and specify that smaller earthquakes obey a Gutenberg-Richter (G-R) distribution of rates on a given fault system. The upper end of this G-R distribution is defined here as $2\sigma_m$ below the smallest mean magnitude of any rupture source on the fault system of interest; this ensures that the exponential-tail and characteristic parts of the frequency-magnitude distribution remain distinct. We note that evidence is scant at best that small earthquakes on individual faults obey G-R statistics, and urge interested users to consider a range of treatments before employing this feature of the code.

Table 4.6. Historical Seismicity and the calculation of F_{small} (see text for explanation).

			Moment Fractions							
Date	**M**	**Moment**	**SAF**	**Hay/RC**	**Calav.**	**Con/GV**	**San G**	**Greenville**	**Mt Diablo**	**Background**
27 Aug 1855	5.50	1.995E+24	2.62E+22	6.08E+23	1.71E+22	4.41E+23	1.11E+22	8.99E+21	1.86E+22	6.512E+23
2 Jan 1856	5.50	1.995E+24	3.31E+23	9.98E+22	2.36E+23	2.32E+22	4.22E+23	2.68E+22	1.54E+22	8.086E+23
17 Apr 1860	5.50	1.995E+24	2.24E+23	3.41E+20	5.81E+23	1.01E+18	4.59E+23	1.22E+21	1.59E+19	7.298E+23
30 Apr 1892	5.50	1.995E+24	2.21E+14	4.71E+20	1.31E+18	2.92E+23	2.70E+13	1.61E+19	1.73E+20	1.703E+24
9 Aug 1893	5.50	1.995E+24	1.16E+22	9.20E+23	6.05E+20	7.93E+22	4.23E+21	9.62E+19	6.43E+20	5.836E+23
2 June 1899	5.50	1.995E+24	3.10E+23	8.45E+23	4.65E+22	1.17E+23	9.99E+22	2.42E+21	2.38E+22	3.025E+23
November 9, 1914	5.50	1.995E+24	8.92E+23	7.59E+21	3.70E+23	9.84E+17	2.75E+23	1.19E+21	2.49E+19	4.487E+23
September 5, 1955	5.50	1.995E+24	0.00E+00	2.52E+14	9.76E+23	0.00E+00	0.00E+00	0.00E+00	0.00E+00	1.019E+24
21 May 1864	5.60	2.818E+24	4.85E+23	1.52E+23	7.73E+23	1.88E+22	2.16E+23	1.34E+23	3.21E+22	9.805E+23
26 Mar 1866	5.60	2.818E+24	5.78E+23	9.21E+20	1.28E+24	4.85E+17	3.08E+23	5.14E+20	4.38E+18	6.539E+23
2 Apr 1870	5.60	2.818E+24	2.59E+23	1.24E+24	2.56E+23	3.56E+23	6.61E+22	3.47E+22	1.24E+23	3.479E+23
31 July 1889	5.60	2.818E+24	2.91E+23	1.62E+24	2.14E+23	1.35E+23	5.11E+22	5.57E+21	7.38E+22	3.394E+23
March 31, 1986	5.60	2.818E+24	0.00E+00	0.00E+00	0.00E+00	0.00E+00	0.00E+00	0.00E+00	0.00E+00	2.818E+24
October 2, 1969	5.60	2.818E+24	0.00E+00	1.76E+21	0.00E+00	0.00E+00	0.00E+00	0.00E+00	0.00E+00	2.817E+24
2 Jan 1891	5.70	3.981E+24	1.44E+24	2.56E+23	1.64E+24	4.05E+20	9.07E+22	2.99E+22	3.90E+21	5.150E+23
August 6, 1979	5.70	3.981E+24	0.00E+00	0.00E+00	7.59E+23	0.00E+00	0.00E+00	0.00E+00	0.00E+00	3.222E+24
October 2, 1969	5.70	3.981E+24	0.00E+00	8.54E+22	0.00E+00	0.00E+00	0.00E+00	0.00E+00	0.00E+00	3.896E+24
15 Feb 1856	5.80	5.623E+24	1.50E+24	1.41E+24	3.63E+23	1.27E+23	5.83E+23	2.20E+22	7.02E+22	1.290E+24
4 July 1861	5.80	5.623E+24	3.04E+23	1.47E+24	1.92E+24	3.13E+23	4.49E+22	4.15E+23	4.50E+23	6.819E+23
17 Feb 1870	5.80	5.623E+24	2.62E+24	1.15E+23	1.10E+24	2.18E+19	6.50E+23	9.10E+21	4.97E+20	1.135E+24
12 Oct 1891	5.80	5.623E+24	1.45E+21	2.89E+24	6.69E+20	1.89E+24	3.00E+20	7.02E+19	2.43E+21	8.158E+23
13 Nov 1892	5.80	5.623E+24	1.67E+24	2.99E+21	1.71E+24	8.85E+16	6.98E+23	9.55E+20	5.29E+18	1.537E+24
March 11, 1910	5.80	5.623E+24	1.55E+24	1.27E+22	1.32E+24	1.28E+19	1.17E+24	2.35E+21	9.56E+19	1.565E+24
January 24, 1980	5.80	5.623E+24	0.00E+00	0.00E+00	0.00E+00	0.00E+00	0.00E+00	3.39E+24	3.95E+23	1.837E+24
26 Feb 1864	5.90	7.943E+24	1.69E+24	5.49E+22	2.24E+24	9.18E+20	1.58E+24	3.00E+22	2.97E+21	2.354E+24
5 Mar 1864	5.90	7.943E+24	1.75E+24	2.54E+23	2.56E+24	1.96E+22	8.75E+23	1.94E+23	3.74E+22	2.237E+24
24 May 1865	5.90	7.943E+24	1.42E+24	3.26E+22	3.48E+24	4.54E+20	8.40E+23	5.55E+22	2.73E+21	2.110E+24
15 July 1866	5.90	7.943E+24	1.57E+23	1.29E+22	1.50E+24	7.84E+21	2.93E+22	1.41E+23	1.03E+22	6.082E+24
28 June 1882	5.90	7.943E+24	3.45E+24	1.00E+23	2.01E+24	6.48E+19	8.08E+23	1.31E+22	7.62E+20	1.562E+24
30 Mar 1883	5.90	7.943E+24	2.11E+24	6.66E+19	3.60E+24	3.43E+12	3.55E+23	7.94E+18	1.88E+15	1.875E+24
30 Apr 1899	5.90	7.943E+24	2.34E+24	2.02E+20	1.50E+24	4.12E+14	1.40E+24	2.48E+19	3.28E+16	2.707E+24
6 July 1899	5.90	7.943E+24	6.74E+23	8.27E+19	5.33E+24	6.02E+14	5.43E+22	1.25E+21	2.69E+17	1.881E+24
19 May 1902	5.90	7.943E+24	2.24E+14	4.94E+20	6.09E+19	1.87E+24	1.80E+13	8.25E+20	7.52E+21	6.063E+24
February 15, 1927	5.90	7.943E+24	1.24E+24	1.39E+20	3.06E+24	1.82E+14	1.20E+24	3.60E+20	9.90E+16	2.451E+24
19 May 1889	6.00	1.122E+25	7.27E+18	1.83E+23	6.91E+23	4.85E+24	3.69E+17	1.03E+24	2.36E+24	2.110E+24
26 Nov 1858	6.10	1.585E+25	2.64E+24	2.84E+24	6.81E+24	9.47E+22	2.61E+23	6.57E+23	2.68E+23	2.254E+24
10 Apr 1881	6.10	1.585E+25	9.36E+21	1.79E+23	2.05E+24	1.13E+22	5.87E+19	2.95E+24	2.08E+23	1.045E+25
26 Mar 1884	6.10	1.585E+25	2.91E+24	2.11E+22	2.27E+24	1.21E+19	5.06E+24	1.34E+22	2.53E+20	5.581E+24
11 June 1903	6.10	1.585E+25	8.27E+24	4.18E+23	4.49E+24	1.37E+18	4.33E+23	7.28E+21	1.85E+20	2.235E+24
3 Aug 1903	6.10	1.585E+25	3.96E+24	2.75E+24	6.81E+24	3.33E+21	1.81E+23	4.19E+22	2.83E+22	2.077E+24
October 22, 1926	6.10	1.585E+25	1.00E+25	1.78E+22	2.73E+24	2.20E+12	3.79E+23	2.28E+20	7.18E+16	2.677E+24
July 1, 1911	6.20	2.239E+25	2.17E+24	3.05E+24	1.52E+25	2.25E+20	8.97E+21	1.84E+23	1.90E+22	1.739E+24
April 24,1984	6.20	2.239E+25	0.00E+00	0.00E+00	2.22E+25	0.00E+00	0.00E+00	0.00E+00	0.00E+00	1.478E+23
24 Apr 1890	6.30	3.162E+25	1.46E+25	7.64E+20	1.19E+25	1.36E+11	2.63E+23	2.44E+19	1.78E+15	4.858E+24
20 June 1897	6.30	3.162E+25	9.92E+24	1.41E+19	1.55E+25	1.43E+07	4.61E+23	7.34E+17	2.73E+12	5.789E+24
31 Mar 1898	6.30	3.162E+25	1.01E+22	1.84E+25	5.20E+22	1.02E+25	1.21E+21	1.41E+21	1.36E+23	2.722E+24
19 Apr 1892	6.40	4.467E+25	8.97E+06	6.27E+18	1.41E+15	4.34E+24	1.35E+05	8.46E+16	1.94E+19	4.033E+25
21 Apr 1892	6.40	4.467E+25	3.31E+06	2.73E+18	7.35E+13	1.51E+24	7.36E+04	4.26E+15	8.16E+17	4.316E+25
10 June 1836	6.50	6.310E+25	1.41E+25	2.01E+23	2.45E+25	6.99E+20	8.42E+24	1.03E+23	4.89E+21	1.578E+25
8 Oct 1865	6.50	6.310E+25	3.56E+25	3.50E+24	1.37E+25	2.51E+19	9.24E+23	4.48E+21	1.39E+21	9.377E+24
June 1838	6.80	1.778E+26	5.80E+25	3.26E+25	4.80E+25	3.15E+23	6.60E+24	8.73E+23	9.99E+23	3.029E+25
21 Oct 1868	6.80	1.778E+26	0.00E+00	1.78E+26	0.00E+00	0.00E+00	0.00E+00	0.00E+00	0.00E+00	0.000E+00
October 18, 1989	6.90	2.512E+26	4.62E+16	0.00E+00	0.00E+00	0.00E+00	0.00E+00	0.00E+00	0.00E+00	2.512E+26
March 21, 1906	7.85	2.85E+27	2.85E+27	0.00E+00	0.00E+00	0.00E+00	0.00E+00	0.00E+00	0.00E+00	0.000E+00
Total moment		4.082E+27								
Threshold **M**			6.65	6.19	5.56	5.95	6.65	5.95	6.4	
MO/yr (**M**<MT)			8.77E+23	1.24E+23	1.48E+22	3.80E+22	1.91E+23	3.01E+22	2.86E+22	4.93E+26
Model Moment/yr			9.815E+24	3.7325E+24	2.49E+24	5.7E+23	3.69E+24	6.57E+23	3.195E+23	2.65915E+24
% of Model			**8.93%**	**3.32%**	**0.60%**	**6.66%**	**5.18%**	**4.59%**	**8.95%**	

Magnitude-frequency distributions for faults

In order to illustrate the long-term seismic behavior of the modeled faults, we calculate the rate of earthquakes as a function of earthquake magnitude. For each realization of the SFBR model, the frequency of earthquake occurrence is calculated at tenth-magnitude increments for each fault, for the background, and for the region as a whole.

The magnitude of each fixed and floating rupture source is described by a pdf, defined above as a truncated normal distribution (**Figure 4.1**). Therefore, we must take into account the probability that each given rupture will or will not contribute to the long-term rate at a given magnitude threshold value M_T:

$$\gamma_{char_i}(\mathbf{M} > M_T) = \sum_{i=1}^{Nrup} \gamma_{char_i} P_i(\mathbf{M} > M_T) \qquad (4.9)$$

where $P_i(\mathbf{M}>M_T)$ is the probability that the magnitude of rupture i is greater than the threshold value, and the summation is made over the suite of *Nrup* fixed and floating rupture sources on the fault of interest. This quantity is evaluated by integrating the pdf from M_T upwards:

$$P_i(\mathbf{M} > M_T) = \int_{M_T}^{\infty} f_{m_i}(m)dm \qquad (4.10)$$

where $f_{\mathrm{mi}}(m)$ is the magnitude probability density function (pdf) for the i^{th} rupture source. This procedure is illustrated schematically in **Figure 4.3**. In that figure, the pdf for Rupture 1 lies entirely below the threshold magnitude M_T, so $P_1(\mathbf{M}>M_T)=0$ and its rate does not contribute to the fault rate at or above this magnitude. The pdf for Rupture 2 lies entirely above M_T, so $P_2(\mathbf{M}>M_T)=1$ and its entire rate contributes to the fault rate. The pdf for Rupture 3 straddles M_T, so $P_3(\mathbf{M}>M_T)$, the ratio of the shaded area to the entire area under the pdf, is found from (4.10).

Earthquake rate for fault segments

It is useful, for comparison with available geologic data, to calculate the rate at which a segment is ruptured by a characterized earthquake. The segment rupture rate is computed by summing the rate of the rupture sources (fixed and floating) that affect the given segment.
The rate of floating earthquakes are distributed uniformly along the rupture (pro-rated to the segments according to length).

The rate at which a fault segment ruptures in earthquakes greater than some threshold level of interest (e.g. $M_T \geq 6.7$) is given by (4.9), where the summation is restricted to those ruptures that involve that fault segment.

Background earthquakes

We use the Gutenberg-Richter form, truncated at high magnitude, to describe the frequency of occurrence of background earthquakes. Historical rates of earthquake occurrence were drawn

from the analysis of Wesson and others [in prep.]. Two G-R relations, log N/yr = *a* - *b*M, that describe the magnitude-frequency distributions of background earthquakes were developed: one for the 1951-1998 period (**M**≥3) with *a*=3.67 [3.60 to 3.74 at 95% confidence] and *b*=0.89; and the other for the 1836-2001 period (**M**≥5.5) with *a*=3.94 [3.62 to 4.31 at 95% confidence] and *b*=0.89.

The 1951-1998 relation provides a rate based on recent activity, and the 1836-2001 relation provides a rate based on longer-term activity. We use both rates to estimate the 30-year conditional probability of **M** ≥ 6.7 earthquakes in the background. That is, we define 2 models, one based on the recent rate of **M** ≥ 6.7 earthquakes and the other on the longer-term rate. Each model is then split into 3 branches, based on the mean rate, the +2σ rate and the -2σ rate. The WG steering committee voted on the relative weights of the 2 models (weights of 0.483 and 0.517, respectively), which were then apportioned across the 6 resulting branches in the calculation sequence (**Table 4.7**).

For this study the maximum magnitude for background earthquakes is 7.25±0.25. For **M**=4.1+logA, **M**7.5 implies A=2500km2, or a fault patch 180x14km. **M**7.25 implies A=1400km2, or a fault patch 100x14km. While thrust fault events on blind faults are likely sources of large background events they, will most likely not exceed **M** 6 1/2-**M**6 3/4, and larger strike-slip events on uncharacterized faults are possible. WG02 has not characterized the strike-slip Bartlett Springs fault, judged capable of producing an **M**7.1 segment-rupturing event (WGNCEP, 1996). If the 85-km-long Bartlett Springs segment ruptured with adjoining segments to the north, an **M**7.25 or perhaps M 7.5 might result. Therefore, a strike-slip "background" events as large as **M**7 .5 might occur in the in the northeast part of the study region. Because the truncated G-R distribution falls off sharply as the maximum magnitude is approached, the rate of background earthquakes above **M**7 is low and their probability extremely small.

Table 4.7. Background earthquake distribution parameters *a* and *b*, and branch weights.

a	*b*	Weight
From 1951-1998 catalog. Group weight 0.483.		
3.60	0.90	0.054
3.67	0.90	0.434
3.74	0.90	0.054
From 1836-2001 catalog. Group weight 0.517.		
3.62	0.89	0.046
3.94	0.89	0.366
4.31	0.89	0.046

Results: Long-term earthquake rates in the SFBR

Each realization of the SFBR model yields one complete characterization of each of the seven fault systems and the rate of background earthquakes. For the results presented herein, we compiled 10,000 realizations, a number sufficient to adequately sample the range of weighted branch choices. For each realization we retained mean values of the rate of failure of each fault segment in characterized (fixed or floating) earthquakes, the mean magnitude and mean rate of failure of each characteristic and floating earthquake source, and the rate and maximum magnitude of background earthquakes. We then noted the mean, median and 95% bounds on the resulting distribution of 10,000 values. Those statistical measures are summarized for the rupture sources and fault segments, respectively, in **Tables 4.8** and **4.9**. For each rupture source listed in **Table 4.8**, the mean magnitude and its rate of occurrence represent rupture of that source by itself. The recurrence intervals for the rupture sources are displayed graphically in **Figure 4.4**. For each fault segment listed in **Table 4.9**, the mean rate represents the rate at which a rupture occurs on that segment, whether or not the rupture initiated in that segment. (In other words, the segment rates are the sum of rates of the rupture sources that affect the segment.)

Table 4.8. Long-term magnitudes and occurrence rates of rupture sources. For reference, recurrence intervals are also listed; these are simply calculated as the inverse of the occurrence rate statistics listed in the center columns.

		Mean magnitude			Occurrence rate (/yr)			Recurrence interval (yr)		
Fault Name	Rupture Source	Mean	2.5%	97.5%	Mean	2.5%	97.5%	Mean	2.5%	97.5%
San Andreas	SAS	7.03	6.84	7.22	0.0007	0	0.0015	1402	646	∞
	SAP	7.15	6.95	7.32	0.0005	0	0.0010	2017	967	∞
	SAN	7.45	7.28	7.61	0.0001	0	0.0008	7180	1316	∞
	SAO	7.29	7.12	7.44	0.0002	0	0.0011	4540	897	∞
	SAS+SAP	7.42	7.26	7.56	0.0010	0.0002	0.0029	1037	343	4863
	SAP+SAN	7.65	7.48	7.79	0	0	0	∞	∞	∞
	SAN+SAO	7.70	7.53	7.86	0.0012	0.0004	0.0035	809	282	2772
	SAS+SAP+SAN	7.76	7.59	7.92	0.00002	0	0.0001	42489	8240	∞
	SAP+SAN+SAO	7.83	7.65	8.01	0.0001	0	0.0004	13046	2676	∞
	SAS+SAP+SAN+SAO	7.90	7.72	8.10	0.0026	0.0012	0.0042	378	239	808
	floating	6.90	6.90	6.90	0.0009	0.0001	0.0019	1104	536	7723
Hayward/RC	HS	6.67	6.36	6.93	0.0034	0.0012	0.0069	292	144	830
	HN	6.49	6.18	6.78	0.0032	0.0011	0.0069	312	146	907
	HS+HN	6.91	6.68	7.12	0.0024	0.0009	0.0047	413	211	1100
	RC	6.98	6.81	7.14	0.0040	0.0023	0.0063	250	159	438
	HN+RC	7.11	6.94	7.28	0.0005	0	0.0013	2086	766	∞
	HS+HN+RC	7.26	7.09	7.42	0.0003	0.0001	0.0007	3524	1511	19158
	floating	6.90	6.90	6.90	0.0003	0.0001	0.0006	3524	1706	7294
Calaveras	CS	5.79	0.00	6.14	0.0075	0	0.0158	134	63	∞
	CC	6.23	5.75	6.68	0.0054	0.0025	0.0097	184	103	397
	CS+CC	6.36	5.87	6.75	0.0018	0	0.0065	541	155	∞
	CN	6.78	6.58	6.97	0.0035	0.0015	0.0065	284	154	685
	CC+CN	6.90	6.68	7.11	0.0001	0	0.0011	10958	924	∞
	CS+CC+CN	6.93	6.72	7.14	0.0006	0	0.0018	1555	543	∞
	floating	6.20	6.20	6.20	0.0030	0.0009	0.0077	331	130	1158
	floating CS+CC	6.20	6.20	6.20	0.0120	0.0025	0.0285	83	35	405
Concord/GV	CON	6.25	5.75	6.67	0.0014	0.0002	0.0038	690	264	5374
	GVS	6.24	5.75	6.65	0.0007	0.0001	0.0018	1527	551	12725
	CON+GVS	6.58	6.13	6.91	0.0005	0.00003	0.0016	2158	640	40002
	GVN	6.02	5.45	6.49	0.0017	0.0002	0.0043	582	231	4474
	GVS+GVN	6.48	6.03	6.81	0.0009	0.0001	0.0024	1125	411	10866
	CON+GVS+GVN	6.71	6.34	7.00	0.0017	0.0003	0.0050	580	199	2888
	floating	6.20	6.20	6.20	0.0026	0.0001	0.0126	386	80	9327
San Gregorio	SGS	6.96	6.75	7.17	0.0007	0	0.0023	1403	444	∞
	SGN	7.23	7.04	7.41	0.0012	0	0.0034	828	295	∞
	SGS+SGN	7.44	7.27	7.58	0.0008	0	0.0021	1202	483	∞
	floating	6.90	6.90	6.90	0.0008	0.0004	0.0014	1220	733	2833
Greenville	GS	6.60	6.37	6.83	0.0010	0.0004	0.0019	976	515	2622
	GN	6.66	6.41	6.88	0.0010	0.0004	0.0018	1040	550	2824
	GS+GN	6.94	6.74	7.13	0.0005	0.0002	0.0009	1994	1063	5393
	floating	6.20	6.20	6.20	0.0002	0.0001	0.0003	5897	3131	15835
Mt Diablo	MTD	6.65	6.42	6.89	0.0026	0.0006	0.0053	389	189	1609

Table 4.9. Long-term earthquake recurrence rates and recurrence intervals for SFBR fault segments. Rates include earthquakes on all fixed and floating rupture sources that affect a given segment. For reference, recurrence intervals are also listed; these are simply calculated as the inverse of the occurrence rate statistics listed in the center columns.

		Recurrence rate (/yr)			Recurrence Interval (yr)		
Fault Name	Segment	Mean	2.5%	97.5%	Mean	2.5%	97.5%
San Andreas	SAS	0.0045	0.0028	0.0064	224	156	363
	SAP	0.0044	0.0027	0.0063	229	160	377
	SAN	0.0045	0.0025	0.0065	223	153	397
	SAO	0.0044	0.0025	0.0065	225	154	405
Hayward/RC	HS	0.0062	0.0035	0.0101	161	99	283
	HN	0.0065	0.0037	0.0105	155	95	273
	RC	0.0049	0.0029	0.0073	205	136	345
Calaveras	CS	0.0134	0.0026	0.0245	75	41	390
	CC	0.0185	0.0094	0.0326	54	31	106
	CN	0.0054	0.0030	0.0085	187	117	339
Concord/GV	CON	0.0046	0.0015	0.0084	219	118	646
	GVS	0.0048	0.0015	0.0089	210	112	665
	GVN	0.0050	0.0016	0.0094	201	106	622
San Gregorio	SGS	0.0019	0.0007	0.0031	540	319	1441
	SGN	0.0026	0.0011	0.0043	392	232	926
Greenville	GS	0.0016	0.0006	0.0030	623	330	1677
	GN	0.0016	0.0006	0.0029	644	343	1748
Mt Diablo	MTD	0.0026	0.0006	0.0053	389	189	1609

Evaluating the SFBR Model

The products of the calculation sequence are a) the mean occurrence rate for earthquakes on 18 fault segments and the 7 characterized faults and b) the mean magnitude and recurrence rate of each rupture source. Adding the mean rupture rate of the background yields a rate for the entire SFBR. While the resulting SFBR model accounts for all $\mathbf{M} \geq 6.7$ events, it does not include all of the $\mathbf{M} < 6.7$ events in the region. How well does the SFBR model work as a physically realistic earthquake machine? There are a number of consistency checks available to evaluate whether the numerical operations in the WG02 calculation sequence produce reasonable results. First, we compare the predicted rate of $\mathbf{M} \geq 6.7$ earthquakes with the historical record back to 1836 and paleoseismic earthquake records back to about 1600. Second, the recurrence rate of $\mathbf{M} \geq 6.7$ events for each fault segment is compared to paleoseismic recurrence rates obtained from trenches excavated across the fault trace within that segment. Finally, regional results from the SFBR model are compared to other regional models.

These model earthquake rates are determined by factors we can loosely describe as "absolute", factors that more or less raise (or lower) the rates uniformly, and "relative", factors that change the rates of earthquakes by changing the distribution of earthquakes with respect to size. The "relative" factors operate differently on different faults, but the sum of the earthquake rates on the faults is the principal determinant of the regional rates.

For the region as a whole, such "absolute" factors include the regional slip rate across SFBR (36 - 43 mm/yr), the weighted **M** - log *A* relations, and the background earthquake rate. For individual faults, the fault-specific slip velocity and the weighted **M** - log *A* relations are also "absolute" factors. Significant "relative" factors operating on individual faults include the weighted fault-rupture models which express the fault's seismogenic character; **M** for the floating earthquake (the larger the floating earthquake, the more seismic moment it releases and the less frequently it occurs); and the seismic slip factor *R*. In this analysis, $R < 1$ reduces fault area *A* for all affected fault segments and rupture sources, thereby reducing the mean magnitudes and increasing the rates of these earthquakes.

Checks on the SFBR model

Regional comparisons

The mean rate of occurrence and magnitude distribution of $\mathbf{M} \geq 6.7$ earthquakes are the two most important model results for evaluating the SFBR model since observations of these quantities were not a part of the model construction. The SFBR model produces 0.031 $\mathbf{M} \geq 6.7$ earthquakes/yr (0.024 to 0.041 at the 95% confidence level), and b=1.02 ± 0.03 (1σ) for $6.7 \leq \mathbf{M} \leq 7.7$ (**Figure 4.5**). The 1.02 slope of the magnitude frequency distribution is greater than the b-value of 0.90 obtained by Bakun (1999) for the SFBR but Bakun's (1999) b-value for the $\mathbf{M} \geq 5.5$ earthquakes since 1850 was 0.99 ± 0.11. The modeled mean rate of 0.031 $\mathbf{M} \geq 6.7$ earthquakes/yr is consistent with that observed since 1836. The observed rate, 0.024 $\mathbf{M} \geq 6.7$ earthquakes/yr, includes only four events; assuming a Poisson model, regional rates of $\mathbf{M} \geq 6.7$ earthquakes lower than 0.007 and greater than 0.047 respectively can be rejected with 95% confidence (Reasenberg et al, 2003). Finally, the $\mathbf{M} \geq 5.5$ historical/instrumental rate of seismicity connects with the SFBR model, both in the vicinity of **M**=6.7 and at larger magnitudes (**Figure 4.5**).

Another regional check is the comparison between the SFBR long-term rates and the regional paleoseismic record. The timing of the most recent rupture associated with a large magnitude earthquake on each of the characterized faults is described in **Chapter 3** and summarized in **Figure 4.6**. The most robust observations of recent rupture are on the San Andreas, northern and southern Hayward, and Rodgers Creek faults, each occurring after 1600 AD. The timing of the most recent event on the northern Calaveras is less certain and its size is also not as well constrained. The most recent event on the San Gregorio fault has large uncertainties but is permissively post-1600. If each of the 10 events shown on **Figure 4.6** is an independent $\mathbf{M} \geq 6.7$ earthquake, then a rate of N($\mathbf{M} \geq 6.7$) of 0.024 events/yr have occurred over the past 400 years. This is the same rate as obtained above for the historical record since 1836. If the San Gregorio event occurred earlier than 1600 and two of the Hayward-Rodgers Creek events represent a combined rupture source, the region would have experienced 8 events during the past 400 years for a rate N($\mathbf{M} \geq 6.7$) of 0.020 events/yr. In either case the paleoseismic record, as presently understood, is in good agreement with both the historical regional seismicity rate and the earthquake production rate of the long-term SFBR model, excluding background earthquakes not yet seen in the paleoseismic record.

Although the San Andreas and Hayward-Rodgers Creek faults are the two principal faults that contribute most significantly to the regional **M** ≥ 6.7 seismicity of SFBR, these faults generate earthquakes in very different ways from each other and from SFBR as a whole. The Hayward-Rodgers Creek fault is composed of three segments, the southern Hayward (HS), northern Hayward (HN) and Rodgers Creek (RC) segments. More than 95% of the model ruptures of the Hayward-Rodgers Creek fault occur either as single-segment ruptures or in the HS + HN combination, all with mean **M** ≤ 7.0 (**Table 4.8**). More than 60% of the ruptures of the San Andreas fault, on the other hand, occur as the 2-segment SAN+SAO or 4-segment SAS+SAP+SAN+SAO ruptures, both with mean **M** ≥ 7.75. These two, very different modes of rupture, with a small contribution from the San Gregorio fault at intermediate magnitudes (7.0 ≤ **M** ≤ 7.4), add up to a G-R regional distribution for 6.7 ≤ **M** ≤ 7.85. That is, another consequence of the SFBR model is the strong asymmetry in the production of more-frequent **M** ≤ 7.0 earthquakes on the East Bay faults, principally the Hayward-Rodgers Creek fault, with respect to the production of less frequent, (**M** ≥ 7.2 earthquakes on the West Bay faults, principally the San Andreas fault.

This East Bay-West Bay asymmetry is due to two features of the model, the shorter segment lengths of the East Bay faults relative to the San Andreas and San Gregorio faults and the expert-opinion assignments of the relative frequency of occurrence of multi-segment ruptures, based on the perceived strength of segment boundaries and site-rupture chronologies. It does not seem likely, for example, that the four known co-seismic ruptures inferred from the paleoseismic record for the southern Hayward segment between AD 1470 and 1868 (Lienkaemper and others, 2002) could involve more than one multi-segment rupture, given the rate at which these events occurred; The first known event, ca. AD 1470, may have been multi-segment rupture and may have followed a long quiescence. Andrews and Schwerer (2000) found the same East Bay-West Bay asymmetry in the production of small and large earthquakes without recourse to expert opinion. Their Figure 4a shows not only this East Bay-West Bay asymmetry, but also nearly the same transition magnitude (at **M** =7.0) produced by the SFBR model.

Figure 4.5 also reveals that the background sources contribute significantly to the SFBR model in the magnitude range 6.7 ≤ **M** ≤ 7.0. The background is based on Wesson el al.'s (2003) analysis of historical seismicity relative to known faults and WG02's expert-opinion assignments of weighted maximum magnitudes for the magnitude-frequency distribution. The uncharacterized faults in SFBR that contribute to the background, with the exception of the Bartlett Springs fault, are not likely capable of producing **M** > 7.0 earthquakes. The rate of background earthquakes accounts for 6% of the potential seismic moment in the SFBR (**Figure 4.5).**

Fault-specific comparisons

The SFBR model is next compared on a fault-by-fault basis to the seismicity of that fault for the past 165 years and to the paleoseismic record of significant earthquakes on that fault, as expressed in trenches excavated across them.

Historical/Instrumental Seismicity Data

The seismicity of the seven characterized faults, the background, and the SFBR as a whole, together with their associated 5% and 95% ranges, are shown in **Figure 4.7**. Seismicity in the

SFBR, even since 1836, is sparse, and sparser still when partitioned onto seven faults and the background. Three general features of the SFBR seismicity are apparent. First, there is general concordance of the **M** ≥ 5.5 seismicity since 1836 (open squares) with the SFBR model rates of **M** ≥ 6.7 earthquakes, at least for the more active San Andreas, Hayward-Rodgers Creek, and Calaveras faults. (There is less agreement for the lower slip-rate faults; the agreement between the model and observed seismicity for the background is predetermined, the model background seismicity being the observed background seismicity.) Second, with the exception of the Greenville fault, the pronounced drop in the regional seismicity rate following the 1906 earthquake is expressed by every source (compare N/yr of pre-1906 open diamonds to post-1906 solid squares in **Figure 4.7**). Third, the 1951 to 1998 seismicity, mostly at **M** ≤ 5.5, is generally disconnected from the SFBR model rates of **M** ≥ 6.7 earthquakes. This discrepant rate for the last several decades is pronounced for the San Andreas and Hayward-Rodgers Creek faults, the two faults that contribute the most to seismicity rates for the SFBR model and for the historical record since 1836.

The Mt. Diablo thrust has no surface expression; its geometry, a 25-kilometer-long WNW-ESE zone dipping to the northeast, is inferred from structural and kinematic models of Mt. Diablo. Although modeled by WGCEP (1996) as an unsegmented plane, the Mt. Diablo thrust likely contains tear faults. Most, if not all, of the recent events that are associated with the Mt. Diablo thrust on **Figure 4.7g** are known by their focal mechanisms to be associated with vertical, east-west striking strike-slip faults (Walter and others, 1998; Wesson and others, 2003) that crosscut the Mt. Diablo thrust.

Paleoseismic Data

Paleoseismic recurrence interval data (**Chapter 3**) are in short supply for SFBR faults, but those values that are available (**Table 4.10**) can be compared to recurrence intervals calculated by the SFBR model. The column "WG02 mean RI" in **Table 4.10** is the frequency of occurrence of all segment-rupturing characteristic earthquakes for that segment (i.e., no **M**6.7 threshold). The 95% confidence range of the model RI are given in parentheses. These recurrence intervals are directly comparable to the trench data (RI Trench), which provide frequency of occurrence of ruptures at a site regardless of whether they represent single or multiple-segment events. The values in the "RI Trench" column are estimates of mean rupture rate based on the number of events and intervals defined in a trench during a measured period of time (**Chapter 3**). The column "RI Calculated" gives average repeat time derived from slip/event divided by the slip rate for those faults for which these data are available.

Table 4.10. Comparing Paleoseismic and SFBR Model Mean Recurrence Intervals (RI) (years)

Fault Segment	SFBR Model Mean RI	RI Trench	RI Calculated
San Andreas (SAN)	223 (153 to 397)	180 to 370	218 (181 to 262))
Southern Hayward	161 (99 to 283)	110 to 170	211 (136 to 328)
Northern Hayward	155 (95 to 273)	270 to 710	--
Rodgers Creek	205 (136 to 345)	235 to 387	230 (131 to 370)
Northern Calaveras	187 (117 to 339)	250 to 850	--
San Gregorio North	392 (232 to 926)	300 to 690	571 (300 to 1250)

Geologic information for the Hayward-Rodgers Creek fault system is the most robust for SFBR faults. Paleoseismic observations on the Rodgers Creek fault (Budding and others, 1991; Schwartz and others, 1992) show the occurrence of three surface-rupturing earthquakes between about AD 1000 and 1776. These three events produced 5.1 to 7.2 m of offset, with slip during the most recent event of 1.8 to 2.3 meters. The trench-based recurrence intervals have large uncertainties but, along with the mean calculated RI of 230 years, are reasonably close to the mean SFBR model rupture rate. On the southern Hayward fault there is evidence for four coseismic ruptures (3 intervals) between AD 1470 and 1868 (Lienkaemper and others, 2002). An average slip of 1.9 meters was estimated from geodetic data for the 1868 earthquake, which ruptured this segment (Yu and Segall, 1998). The horizontal offset for older events is not known. Both the paleoseismic (trench) recurrence and the calculated recurrence intervals (average slip in 1868 divided by the 9 ± 2 mm/yr slip rate) are shorter than, but within the uncertainties of, the recurrence intervals predicted by the SFBR model.

The geologic recurrence interval of 270 to 710 years for the northern Hayward fault is based on observations at the Mira Vista site (**Chapter 3**, **Figure 3.1**) of at least four to seven surface-faulting events that occurred during the past 1630 to 2130 years). The event history is likely incomplete at the Mira Vista site because slip can occur here along the main creeping trace without producing brittle deformation in the associated sag pond deposits and short depositional hiatuses in the pond stratigraphic section can also mask event occurrence. The actual rupture rate on the northern Hayward, therefore, is likely to be shorter than the 270 to 710 year trench RI shown in **Table 4.10**. Note that the mean M of HN segment rupturing events is 6.18, too small to be reliably detected in trench excavations. The NH model RI, therefore, cannot meaningfully be compared with the trench results. No horizontal offset data/event are available at the Mira Vista site for use in calculating a slip-based recurrence interval.

Recurrence data for the North Coast segment of the San Andreas fault are sparse but are also in general agreement with WG02 mean rupture rates. Schwartz and others (1998) suggest the penultimate event dates from AD 1630 to 1660. A broader age range, AD 1600 to 1670, is permissive and 235 to 300 years between it and 1906 is reasonable. Based on buried peats at Bolinas lagoon, Knudsen and others (1999) have interpreted the third event back on this segment of the fault to have occurred between AD 1290 to 1340, providing an interval of 390 to 370 years between it and the penultimate event. The intervals for the two surface rupturing events on the SAN segment before 1906 average 298 years. Noller and others (1993) calculate a recurrence

interval of 300 to 350 years in trenches at Ft. Ross, and Prentice (1989) concludes that intervals between large ruptures along this part of the fault range from 188 to 340 years, averaging about 260 years.

On the northern San Gregorio fault at Seal Cove (**Chapter 3**, **Figure 3.8**), Simpson and others (1998) found evidence for two large surface faulting events in the AD 600 to AD 1380 year period. They estimated lateral slip of 5 (3 to 11) m for the most recent event and 3 (±0.2) m for the penultimate event. The SFBR model mean rupture interval for the northern San Gregorio segment is within the range of repeat times estimated from the limited paleoseismic data and an average recurrence interval calculated from the slip per event and a slip rate of 7 ± 3 mm/yr.

At Leyden Creek on the northern Calaveras fault (Chapter 3, **Figure 3.8**) Kelson et al. (1996) identified 5 to 6 surface-rupturing earthquakes during the past 2500 years or so, yielding a recurrence interval of 250 to 850 years. No measurement of horizontal slip per event is available at the site. The SFBR model mean RI of 187 years is outside the range of observed recurrence intervals but the 95% confidence ranges of the model RI and observed RI overlap.

Comparison of the SFBR model to other models

Comparison with Andrews and Schwerer (2000)

Andrews and Schwerer (2000) found frequencies of events in Northern California by fitting to two types of truncated G-R distributions for the region as a whole. Here we compare to their cutoff model, in which the cumulative G-R distribution is cut off abruptly at a maximum magnitude. The associated differential distribution has a spike at the maximum magnitude, so there is a characteristic earthquake component (see Figure 1 in Field and others, 1999). They find that the frequency of events within or partly within the SFBR with **M** > 6.7 is 0.0378 /yr. They assume b=0.9 and use $\mathbf{M}_{max}$=7.77, the magnitude of the 1906 event using the Wells and Coppersmith (1994) magnitude-area relationship. For given total moment release rate, the a value of the distribution varies with maximum magnitude, decreasing by 0.6 for a unit increase in $\mathbf{M}_{max}$. If $\mathbf{M}_{max}$ in the Andrews and Schwerer (2000) model is increased by 0.14 to equal the Working Group's mean **M** for repeats of the 1906 source, then their a value decreases by 0.084, and the frequency of events with **M** > 6.7 becomes 0.0312/yr. They assumed a long-term regional slip rate of 39 mm/yr, all of which was released seismically. If only 36 mm/yr is released seismically, then the rate for **M** > 6.7 becomes 0.029/yr. This result does not depend on details of the Andrews and Schwerer model, but only on the total moment rate, the b value, $\mathbf{M}_{max}$, and the assumed shape of the distribution (the cutoff model).

The frequency of events with **M** > 6.7 on modeled faults in the SFBR model is 0.031/yr. The close agreement with the result in the previous paragraph is only a coincidence, because Andrews and Schwerer used slightly different seismogenic depths, and there is ambiguity about counting events that are partly outside the SFBR. In the Andrews and Schwerer (2000) model, large events predominate on the San Andreas fault and single-segment events predominate on the East Bay faults, in qualitative agreement with the features of the SFBR model described above.

Comparison of rate with formulas for various distributions

A different comparison can be made using the WG02 total moment rate in the following formula, which applies to the truncated incremental ("cutoff") distribution. This is equation (18) in Andrews and Schwerer (2000) and equation (9) in Molnar (1979).

$$N = (1\text{-}B)\,[\,M_0' / M_{0\max}\,]\,[\,M_0 / M_{0\max}\,]^{-B} \qquad (2.13)$$

Where N is the rate of occurrence of events with moment greater than M_0 , B =(2/3)b , $M_{0\max}$ is the moment of the maximum size event, and M_0' is the total long-term moment release rate of the region. We use the following values: B=0.6, $M_{0\max}$=0.82x10^{28} dyne-cm (corresponding to $\mathbf{M}_{\max}$=7.91), and M_0=1.26x10^{26} dyne-cm (corresponding to **M**=6.7). The total moment rate is M_0'=4.72 x10^{25} dyne-cm/yr. Then the formula for the truncated incremental distribution given above predicts N(**M**>6.7)=0.028/yr. Analogous formulas for the truncated cumulative ("roll-off") and gamma distributions (equations 16 and 14 of Andrews and Schwerer) predict rates of 0.043/yr and 0.045/yr respectively. The rate of the SFBR model, N(**M**>6.7)=0.031/yr, is much closer to the rate predicted by the cutoff distribution than to that of the roll-off or gamma distributions. This means that the distribution of events, neglecting background, chosen by WG02 closely fits a cumulative G-R distribution with b=0.9 and having an abrupt cutoff at $\mathbf{M}_{\max}$=7.91.

Comparison of the SFBR rate with Ward (2000)

Ward (2000) simulated seismicity in northern California by modeling the San Andreas fault system as a system of dislocations in a thin elastic plate. His cumulative distribution of event sizes for **M** > 6 closely fits a G-R distribution with b=1.1 and with a rather abrupt cutoff near $\mathbf{M}_{\max}$=7.75. He designed his model to start with the 1906 event having **M**=7.9. Subsequent modeled events on the same length of fault had smaller magnitudes, averaging 7.7. His maximum magnitude could be adjusted by changing the friction parameters. Excluding events on the Maacama fault (outside the SFBR), his rate for events with **M** > 7 is 0.016/yr. The corresponding rate from the SFBR model is N (**M**>7)=0.010/yr. The discrepancy arises from the different values of b and $\mathbf{M}_{\max}$.

Comparison of the WG99 rate to a truncated ("roll-off") G-R model

WG02's fault characterization model, consisting of specified fault segments that rupture either alone or in contiguous combinations, is but one possible model for earthquakes in the SFBR. Alternate models, such as one without segmentation, or one in which non-integer segment ruptures are allowed, were not considered by WG02, but have been previously proposed for the SFBR and other regions (e.g., Jackson, 1996; Andrews and Schwerer, 2000). Here, we compare the SFBR model with a moment-balanced, truncated G-R model for earthquakes on the characterized faults. This model is similar, at least in spirit, to Jackson (1999).

To define a moment-balanced G-R model, we specify a b-value and a maximum magnitude, M_{Max}, that truncates the incremental magnitude-frequency distribution. Historical seismicity for the SFBR (Bakun, 1999) allows us to confine our exploration of G-R models to those with b=0.9. We compare the SFBR model to truncated G-R models for each characterized fault in the SFBR with b=0.9 and M_{Max}=8.25 (**Figure 4.8**). These are "roll-off" models in the terminology of

Andrews and Schwerer (2000). On each fault, the moment release rate (and thus, the a-value) in this G-R model is determined by the fault's slip rate. The regional magnitude-frequency distributions for the G-R and SFBR models are similar, and both closely match the observed rate for **M**≤6.7 earthquakes since 1836. Corresponding G-R models with M_{Max}=8.0 and 8.5 (not shown in **Figure 4.8**) lie approximately 20% above and below the M_{Max}=8.25 curve, respectively.

While this G-R model adequately matches both the observed rates, the two models differ significantly on individual faults. Because the G-R model lacks characteristic earthquakes, its rate of **M**~7.8 earthquakes on the San Andreas fault is about 2/3 of that for the SFBR model, which assigns significant weight to the occurrence of 1906-type rupture sources (Chapter 4). In order to balance the moment release rate on this fault, the G-R model has higher rates of **M**≤7.2 earthquakes than the SFBR model by a factor of approximately 2~3. Observed rates on the San Andreas fault since 1836 (red triangles in **Figure 4.8**) are close to those in the SFBR model, but are about a factor of 3 below the rate in the G-R model. (For example, the G-R model includes the occurrence of one **M**≥6 earthquake on the San Andreas fault per decade, on average, while approximately 5 have occurred in the past 16 decades in the SFBR. This estimate is not an integer because it derives from the Wesson et al.'s (2003) association method.)

On the Hayward-Rodgers Creek, Calaveras and Concord-Green Valley faults, the G-R model assigns more weight to **M** ≥ 7.2 earthquakes than does WG02, owing to the application of $\mathbf{M}_{Max}$=8.25 on each fault. In order to balance the moment rate on these faults, the rate of **M**≤6.7 earthquakes in the G-R model is lower than that in the SFBR model. Observed rates since 1836 on the Hayward-Rodgers Creek, Calaveras, and Concord-Green Valley faults are within a factor of two of the SFBR model, but are systematically under-predicted by the G-R model. For example, the G-R model includes the occurrence of one **M**≥6 earthquake every 2 centuries on the Calaveras fault, on average, while perhaps 6 or 7 have occurred in the past 165 years.

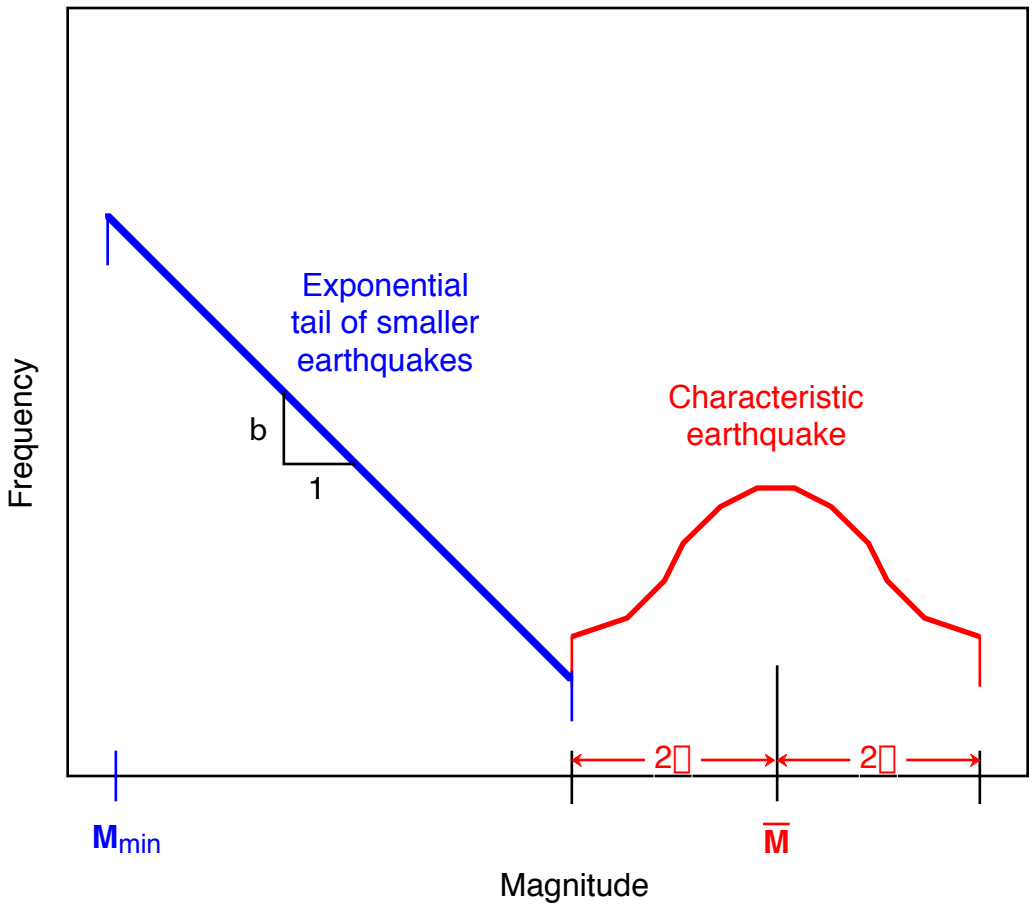

Figure 4.1. Illustration of a magnitude pdf (probability density function) for a WG99 fault containing a single rupture source. The characteristic rupture (which breaks the entire seismogenic area of the source) has a mean magnitude and a natural variability about that mean defined by +/- two standard deviations (where sigma = 0.12). A portion of the moment rate of the fault is expended in an exponential distribution of smaller earthquakes, where the exponential is defined by a b value and magnitude bounds as shown.

Figure 4.2. Comparison of candidate relationships between rupture area (LxW in km) and moment magnitude. Data from Tables E.1-E.4 of Appendix D. Lines correspond to numbered equations in the text, as noted.

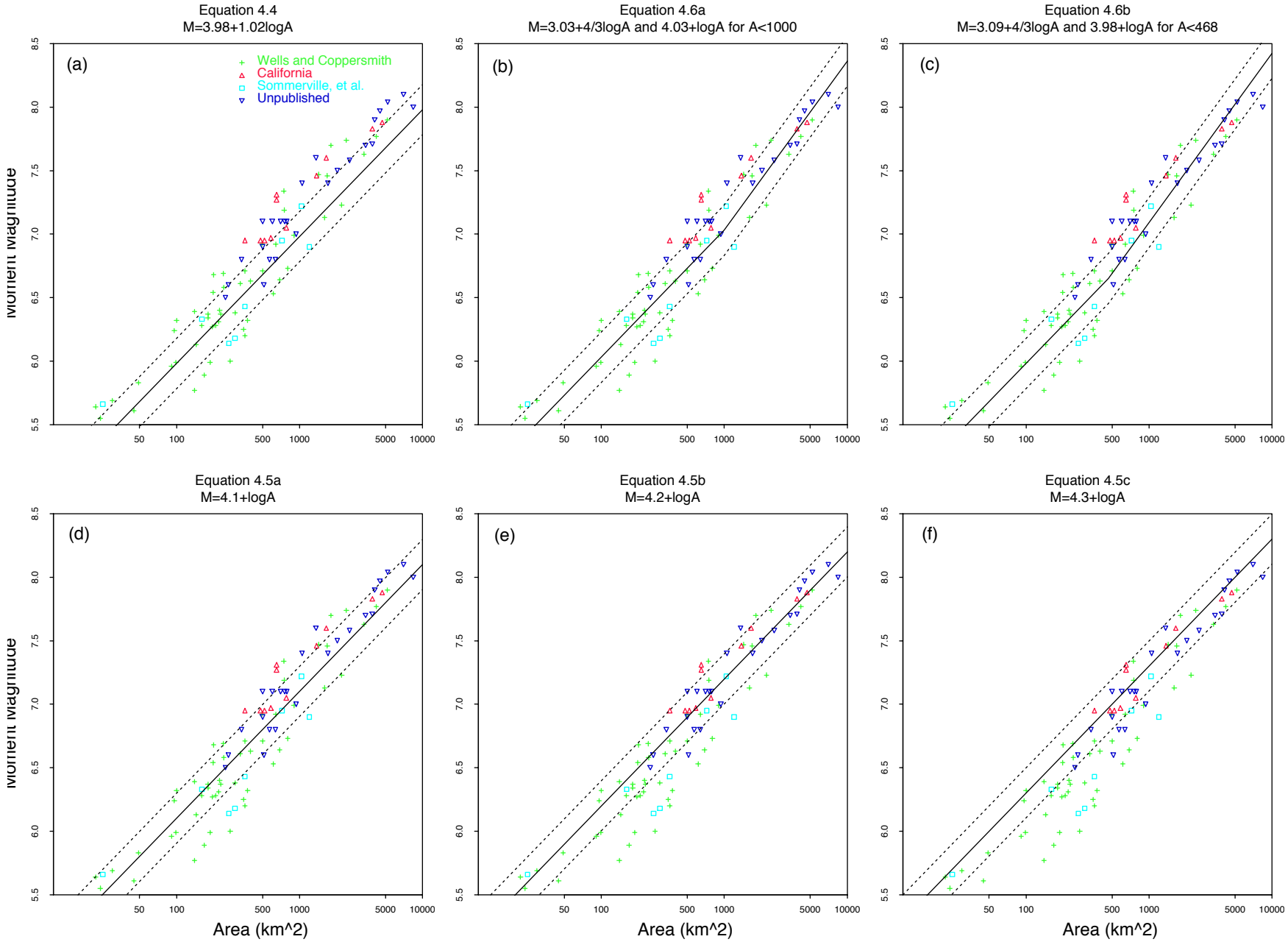

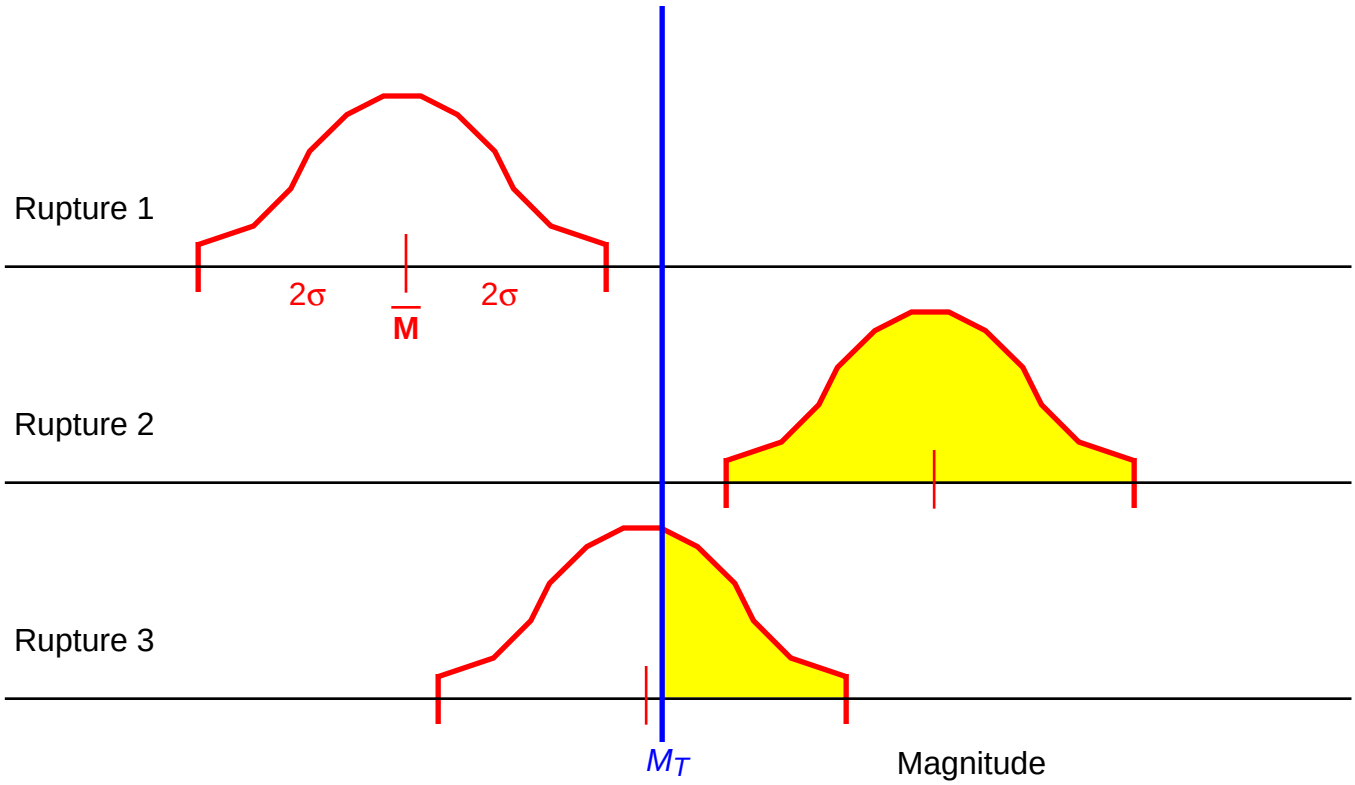

Figure 4.3. An illustrative example of how the WG99 calculation sequence applies a magnitude threshold to three rupture sources with different mean magnitudes. The probability that Rupture 3 will produce an earthquake above magnitude M_T is the ratio of area above M_T to the entire area under the truncated Gaussian (i.e., 0.0 in the first case, 1.0 in the second case, and ~0.4 in the third case).

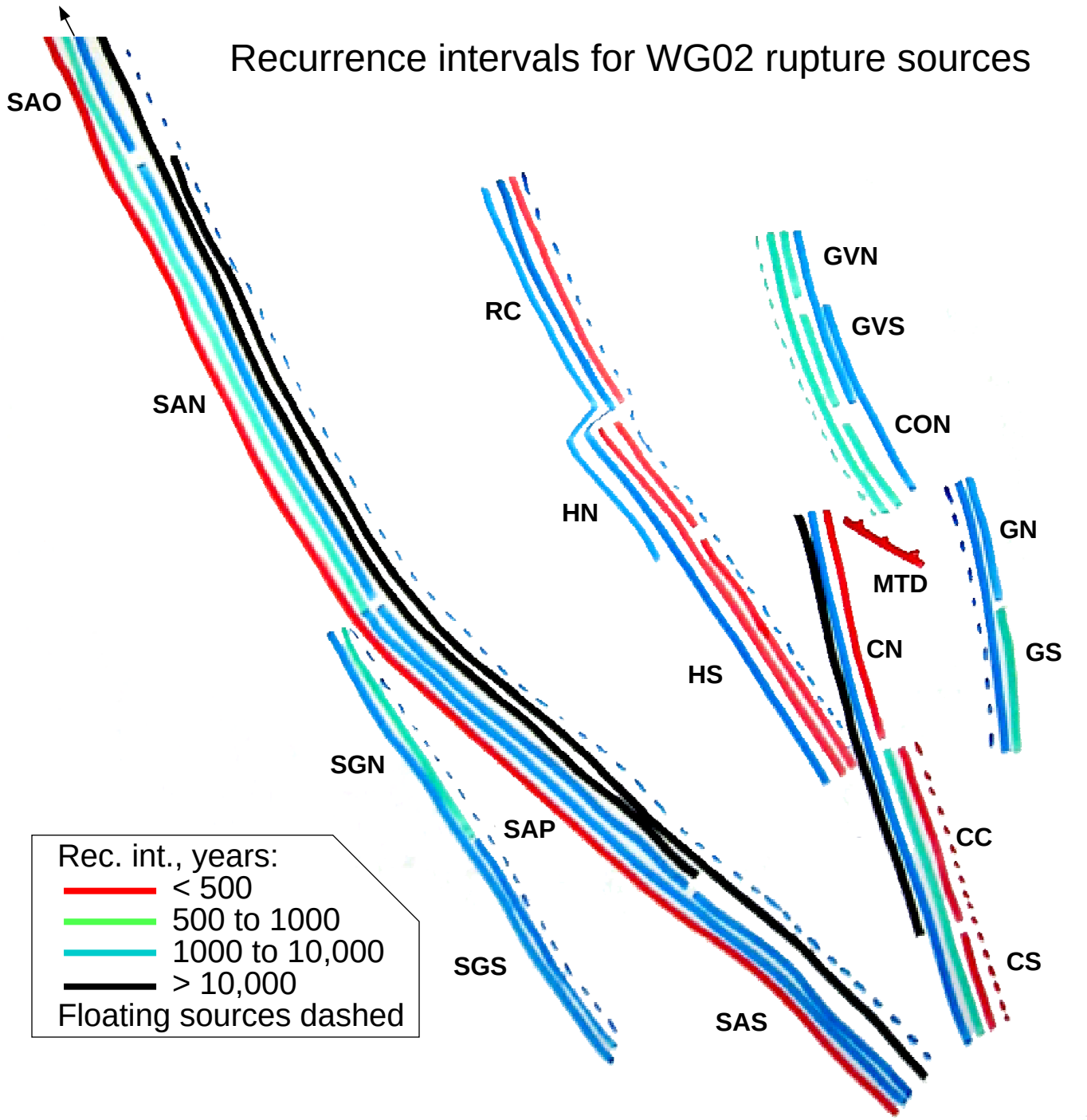

Figure 4.4. Sketch map of SFBR characterized faults, color-coded to indicate long-term recurrence interval of rupture sources. Multiple, parallel curves show the various rupture sources. Floating rupture sources may occur anywhere along the dashed curves.

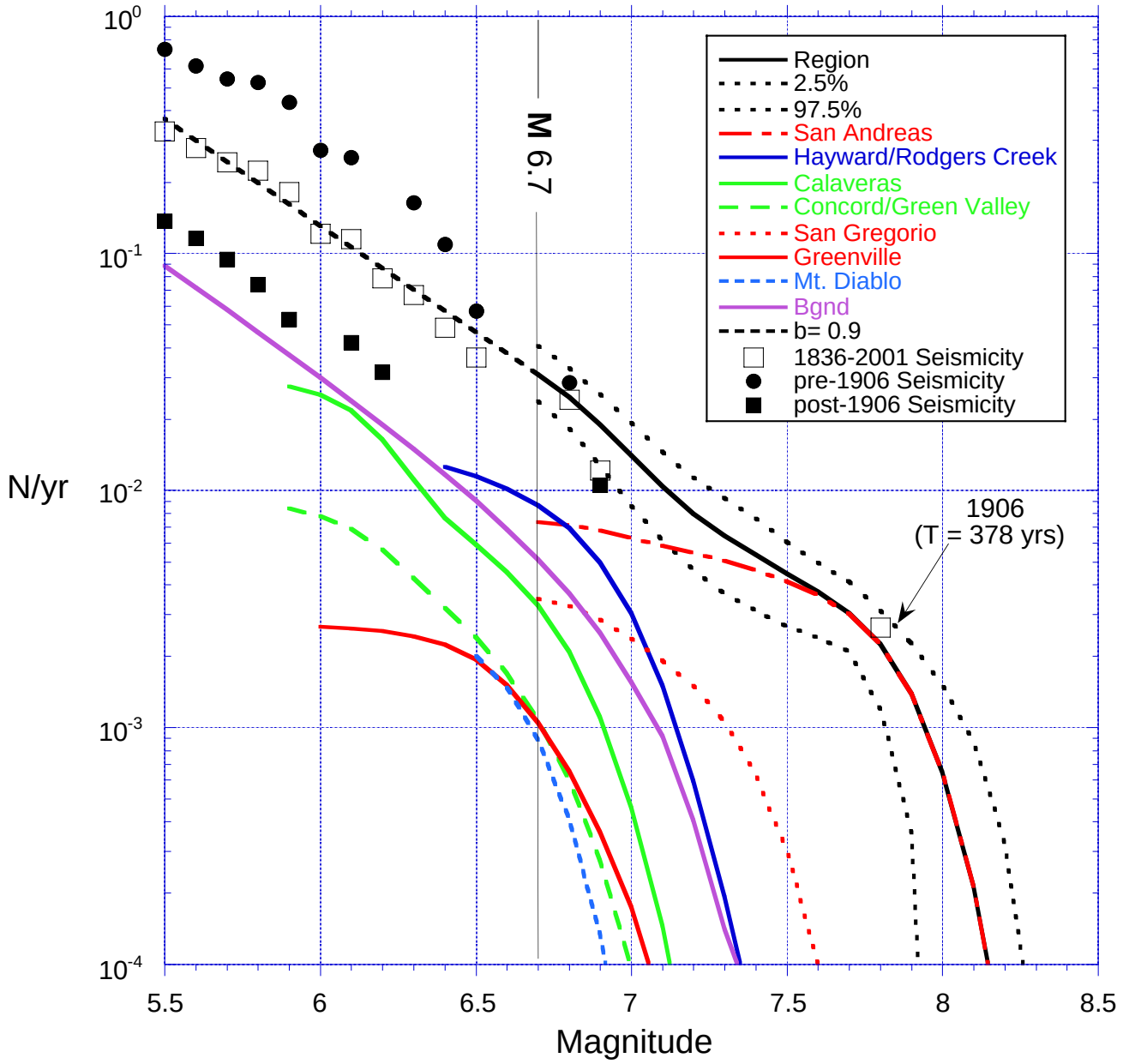

Figure 4.5. Long-term cumulative magnitude-frequency distribution for the SFBR earthquake model. The solid black curve (**M** ≥ 6.7) represents the mean magnitudes for the defined rupture sources, and the dotted black lines are the 95% confidence range. The dashed black line (slope b = 0.9) defines the magnitude distribution for **M** < 6.7 for the region (see text). The 1836-2001 **M** ≥ 5.5 historical seismicity (Bakun, 1999) is plotted as open black squares. The 1906 event is shown with the SFBR model's mean recurrence interval of 378 years for the 1906 rupture source. The pre-1906 and post-1906 seismicity are shown as solid black dots and squares respectively, illustrating the significant impact of the 1906 earthquake on the rates of historical and instrumental seismicity in the SFBR.

The colored curves represent the mean magnitudes of the rupture sources of the characterized faults and the background. The magnitude-frequency distributions of the characterized faults have been constructed with about 6% of the available seismic moment to occur as earthquakes in smaller earthquakes (the exponential tail).

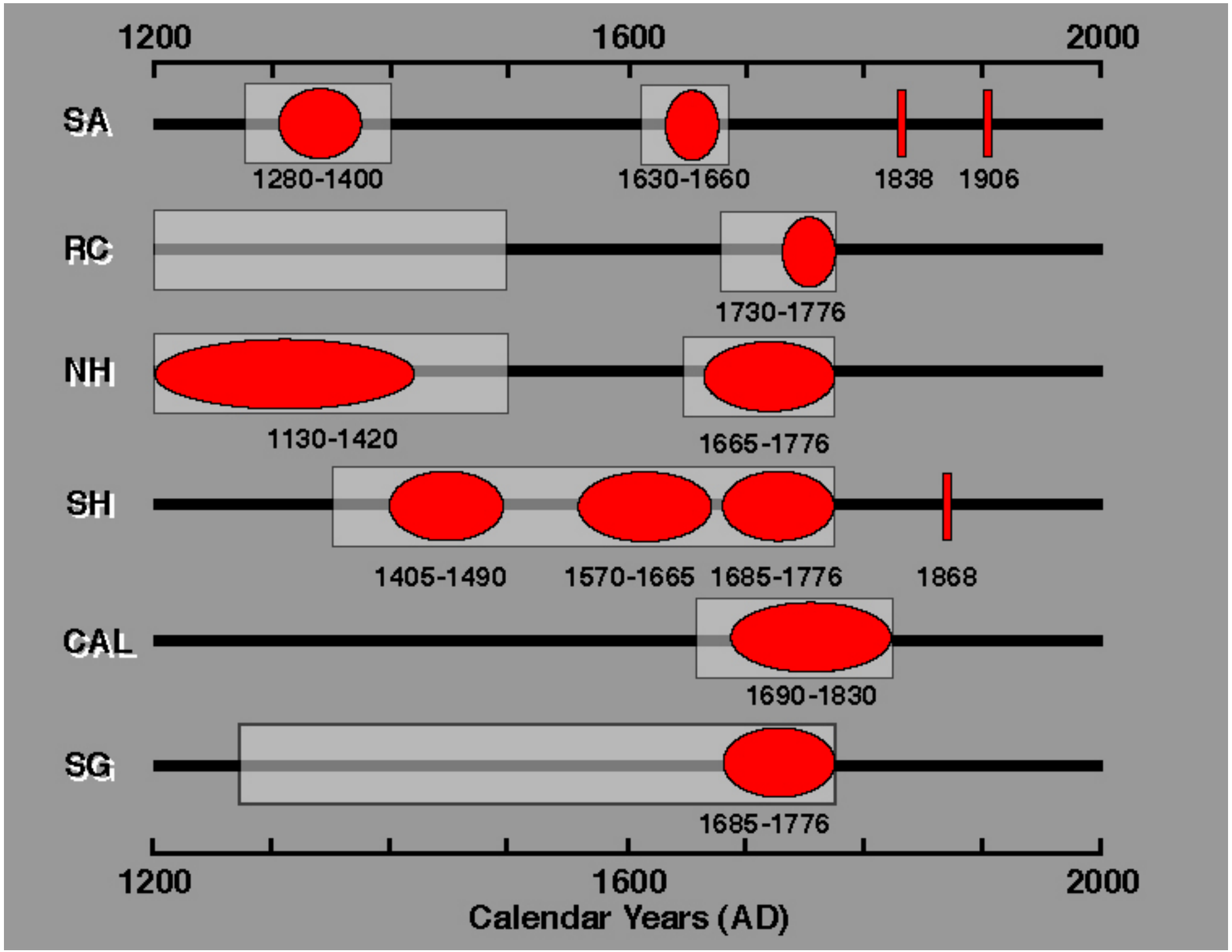

Figure 4.6. Timing of large earthquakes on SFBR faults. Historical events are shown in yellow; timing of prehistoric events as constrained by paleoseismic data and completeness of the historical record are depicted by rectangles and ovals. Rectangles show 2-sigma (95%) uncertainties on event age; ellipses are 1-sigma uncertainties. Data are described in Chapter 3.

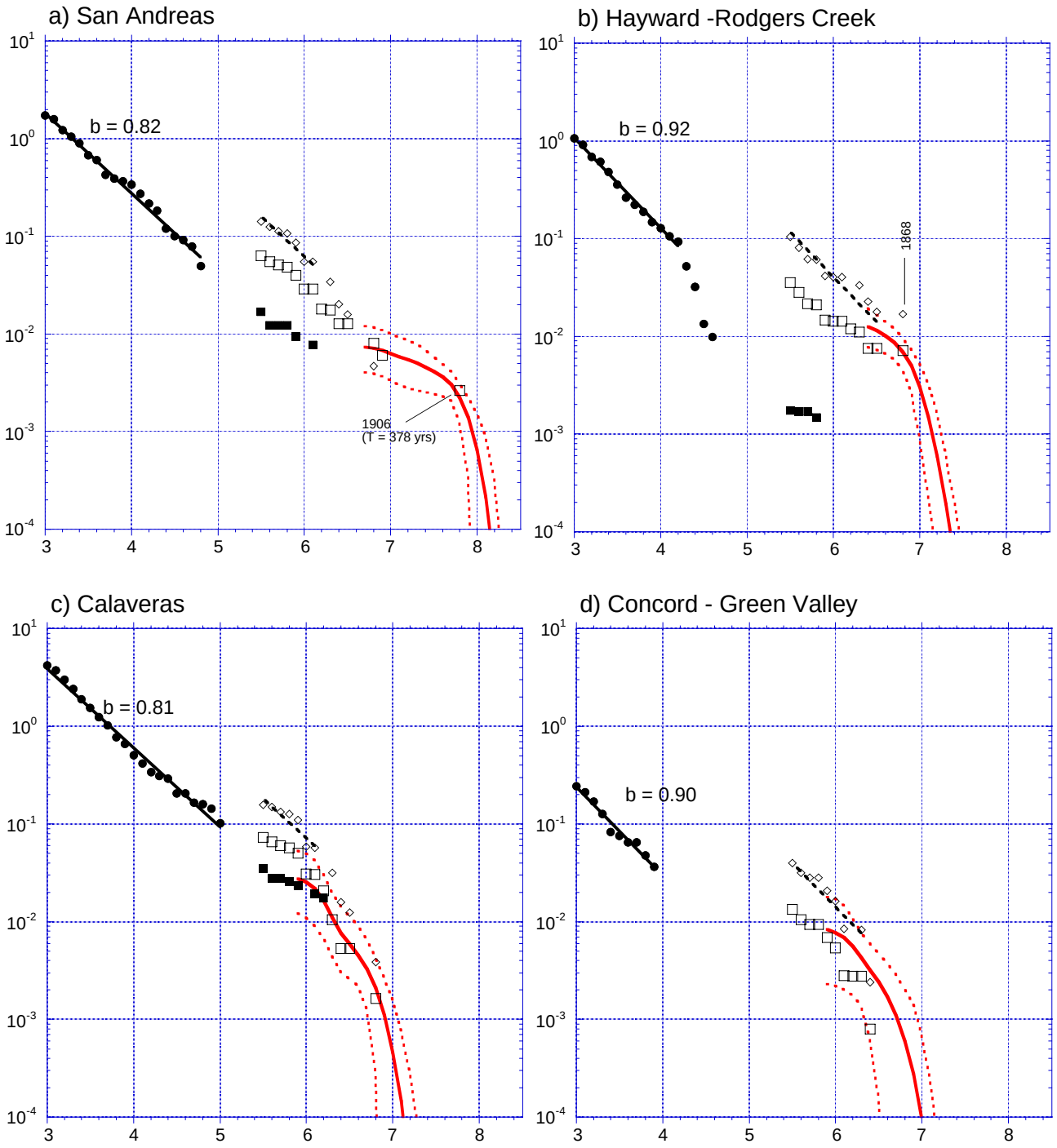

Figure 4.7. Details of the SFBR earthquake model. The solid red curves are the mean magnitudes of the rupture sources for 10,000 model realizations and the dotted red curves represent the 95% bounds.Black symbols are the historical seismicity, using Wesson et al's (2002) fault associations: **M** ≥ 5.5 for 1836-2001 (open squares); declustered 3 ≤ **M** ≤ 5 for 1951-1998 (solid circles); post-1906 **M** ≥ 5.5 (solid squares); pre-1906 **M** ≥ 5.5 (open diamonds).

The solid black line is the least-squares fit of selected 1951-1998 rates to log N/yr = a - b***M**. For the the most active faults, the line is a reasonable fit to the post-1906 **M** ≥ 5.5 rates as well. The dashed black curve is a least squares fit to selected pre-1906 rates, but with b fixed for that fault. The a values apparent for the pre-1906, the post-1906, or the 1836-2001 rates do not represent the SFBR earthquake model, although the 1836-2001 rates are fortuitously about equal the long-term rate. These data suggest how the 6% of the seismic moment at smaller **M** might be distributed for hazard calculations. For each source, the solid red curve defines the magnitude distribution for large events, while 6% of the total moment should be distributed at smaller **M** with a value of b appropriate for that fault.

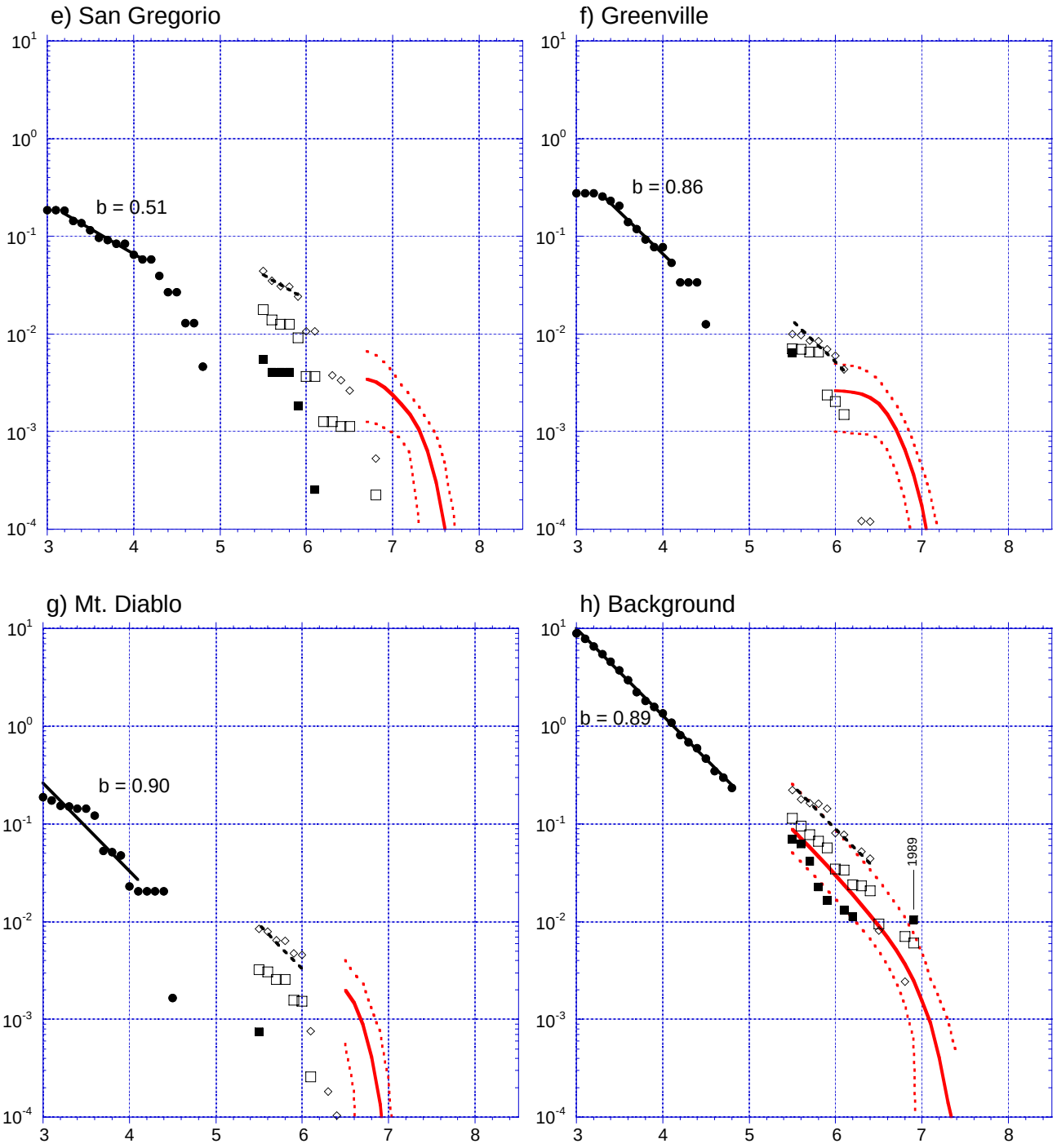

Figure 4.7. continued.

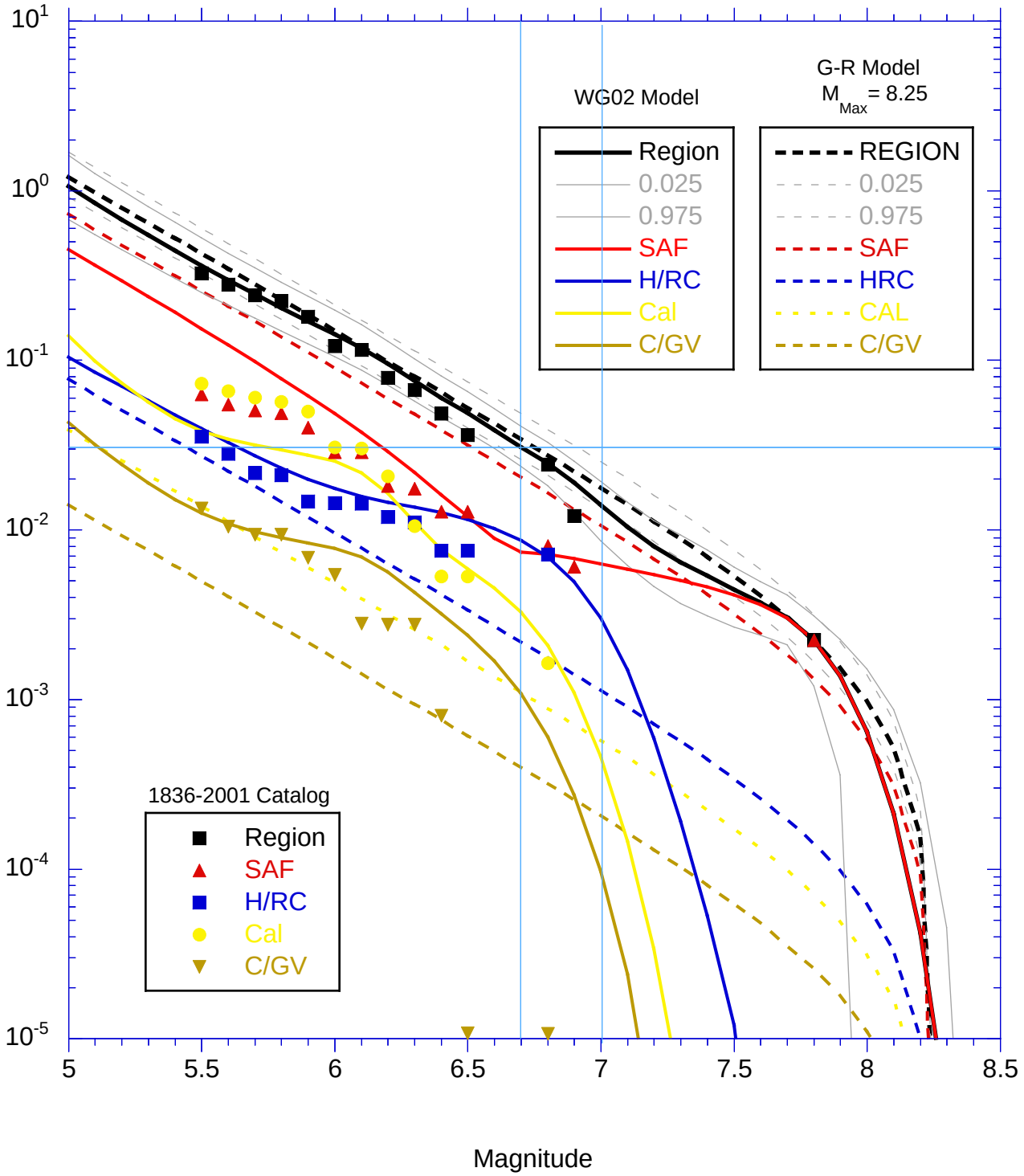

Figure 4.8. Comparison of Gutenberg-Richter and WG02 models to observed rates of earthquakes 1836-2001. Gutenberg-Richter model is the "roll-off" type, truncated at M_{Max}=8.25.